

**Key Points:**

- Cloud occurrence is underestimated below 3 km in ERA5, JRA55, and MERRA2 reanalyses relative to observations, leading to cloud fraction biases
- Observed cloud occurrence is more strongly impacted by weather state than season; ERA5 simulates this pattern better than JRA55 and MERRA2
- Supercooled liquid cloud derived from ceilometer data have higher occurrences than the three reanalyses, with MERRA2 having the least bias

**Correspondence to:**

A. J. McDonald,  
adrian.mcdonald@canterbury.ac.nz

**Citation:**

McDonald, A. J., Kuma, P., Panell, M., Pettersson, O. K. L., Plank, G. E., Rozliaiani, M. A. H., & Whitehead, L. E. (2025). Evaluating cloud properties at Scott Base: Comparing ceilometer observations with ERA5, JRA55, and MERRA2 reanalyses using an instrument simulator. *Journal of Geophysical Research: Atmospheres*, 130, e2024JD041754. <https://doi.org/10.1029/2024JD041754>

Received 6 JUN 2024

Accepted 23 DEC 2024

**Author Contributions:**

**Conceptualization:** A. J. McDonald  
**Data curation:** A. J. McDonald, M. Panell, O. K. L. Pettersson, G. E. Plank  
**Formal analysis:** A. J. McDonald, M. A. H. Rozliaiani  
**Funding acquisition:** A. J. McDonald  
**Investigation:** A. J. McDonald, M. Panell, O. K. L. Pettersson, G. E. Plank, M. A. H. Rozliaiani  
**Methodology:** A. J. McDonald, P. Kuma, L. E. Whitehead  
**Project administration:** A. J. McDonald  
**Resources:** A. J. McDonald

© 2025. The Author(s).

This is an open access article under the terms of the Creative Commons Attribution-NonCommercial-NoDerivs License, which permits use and distribution in any medium, provided the original work is properly cited, the use is non-commercial and no modifications or adaptations are made.

## Evaluating Cloud Properties at Scott Base: Comparing Ceilometer Observations With ERA5, JRA55, and MERRA2 Reanalyses Using an Instrument Simulator

A. J. McDonald<sup>1</sup> , P. Kuma<sup>2</sup> , M. Panell<sup>1</sup>, O. K. L. Pettersson<sup>1</sup> , G. E. Plank<sup>1</sup> , M. A. H. Rozliaiani<sup>1</sup>, and L. E. Whitehead<sup>3</sup> 

<sup>1</sup>School of Physical and Chemical Sciences, University of Canterbury, Christchurch, New Zealand, <sup>2</sup>Department of Meteorology (MISU), Bolin Centre for Climate Research, Stockholm University, Stockholm, Sweden, <sup>3</sup>Department of Geosciences, University of Oslo, Oslo, Norway

**Abstract** This study compares CL51 ceilometer observations made at Scott Base, Antarctica, with statistics from the ERA5, JRA55, and MERRA2 reanalyses. To enhance the comparison we use a lidar instrument simulator to derive cloud statistics from the reanalyses which account for instrumental factors. The cloud occurrence in the three reanalyses is slightly overestimated above 3 km, but displays a larger underestimation below 3 km relative to observations. Unlike previous studies, we see no relationship between relative humidity and cloud occurrence biases, suggesting that the cloud biases do not result from the representation of moisture. We also show that the seasonal variation of cloud occurrence and cloud fraction, defined as the vertically integrated cloud occurrence, are small in both the observations and the reanalyses. We also examine the quality of the cloud representation for a set of weather states derived from ERA5 surface winds. The variability associated with grouping cloud occurrence based on weather state is much larger than the seasonal variation, highlighting weather state is a strong control of cloud occurrence. All the reanalyses continue to display underestimates below 3 km and overestimates above 3 km for each weather state. But the variability in ERA5 statistics matches the changes in the observations better than the other reanalyses. We also use a machine learning scheme to estimate the quantity of supercooled liquid water cloud from the ceilometer observations. Ceilometer low-level supercooled liquid water cloud occurrences are considerably larger than values derived from the reanalyses, further highlighting the poor representation of low-level clouds in the reanalyses.

**Plain Language Summary** This study compares cloud observations from a CL51 ceilometer at Scott Base, Antarctica, with data from three weather reanalyses: ERA5, JRA55, and MERRA2. We used a lidar simulator to better match the reanalyses data with the ceilometer's measurements. The reanalyses slightly overestimate cloud presence above 3 km, but significantly underestimate it below 3 km compared to the ceilometer data. Both the observations and reanalyses show only small seasonal changes in cloud presence. However, grouping the data by weather patterns shows that these patterns strongly influence cloud presence. The reanalyses still underestimated cloud presence below 3 km and overestimated it above 3 km for all weather patterns, but ERA5 data matched the observed changes better than the other reanalyses. We also used machine learning to estimate the amount of supercooled liquid water clouds from the ceilometer data. The ceilometer detected many more low-level supercooled liquid water clouds than the reanalyses simulations, highlighting that issues with the representation of low-level clouds in these models are widespread.

### 1. Introduction

Clouds are fundamental to the Earth's energy balance, influencing surface temperature by reflecting solar radiation, trapping, and emitting infrared radiation. But comparisons between observations and simulations reveal significant biases in the representation of clouds. In particular, large biases were identified over high latitudes in the Coupled Model Intercomparison Project Phase 3 (CMIP3) models (Trenberth & Fasullo, 2010). Subsequent work has made improvements in the simulation of clouds and their properties, but biases are still large and can contain compensating errors which can hide problems (Kuma et al., 2023; A. J. Schuddeboom & McDonald, 2021). Identifying biases' sources is crucial, with previous studies identifying that both insufficient cloud cover and problems with the quantity of supercooled water clouds simulated contribute to biases. The latter issue is a problem because liquid water cloud reflects more shortwave radiation than ice clouds containing the same amount of water (Vergara-Temprado et al., 2018). In particular, models often struggle to simulate supercooled

**Software:** A. J. McDonald, P. Kuma, O. K. L. Petterson, M. A. H. Rozliaiani, L. E. Whitehead

**Validation:** A. J. McDonald

**Visualization:** A. J. McDonald

**Writing – original draft:** A. J. McDonald

**Writing – review & editing:**

A. J. McDonald, P. Kuma, M. Panell, O. K. L. Petterson, G. E. Plank, L. E. Whitehead

liquid water clouds accurately leading to significant shortwave radiation biases (Bodas-Salcedo et al., 2016; Kay et al., 2016; Kuma et al., 2020). These clouds which occur between the 0°C isotherm and the -38°C isotherm, used to represent the homogeneous freezing level, are very common over the Southern Hemisphere (Hogan et al., 2004), the Southern Ocean (Bodas-Salcedo et al., 2016; Kuma et al., 2020), and Antarctica (Listowski et al., 2019). For example, Listowski et al. (2019) identified that the fraction of supercooled liquid-water containing cloud (SLCC) was of the order of 0%–35% over the Antarctic continent. These issues are important because Zelinka et al. (2020) highlighted that changes in the global effective climate sensitivity (ECS) between CMIP Phase 5 and 6 models could largely be attributed to changes in the representation of extratropical Southern Hemisphere clouds.

Observational data on cloud properties at southern high latitude sites is thus an important constraint on ECS and the representation of clouds. Satellite observations offer the most spatially complete constraints for models and also often provide the longest records above the Southern Ocean and Antarctica. They also have a relatively long history of usage as detailed in Lachlan-Cope (2010) and Bromwich et al. (2012). Satellite data have provided valuable insights on cloud cover, cloud phase, seasonality, and the vertical distribution of clouds across the Antarctic continent (Adhikari et al., 2012; Bromwich et al., 2012; Verlinden et al., 2011). However, they do have a number of limitations. In particular, passive satellite sensors face challenges in cloud identification due to the similarity of the properties of snow- and ice-covered ground to low-level cloud (Frey et al., 2008). Additionally, low-level cloud layers and cloud base height observations by satellite instruments are severely limited by the presence of an almost continuous cloud cover in the Southern Ocean which acts to obscure these clouds. Additionally, passive satellite data sets, such as the Moderate Resolution Imaging Spectroradiometer (MODIS; Platnick et al., 2003) data set and the data used in the International Satellite Cloud Climatology Project (ISCCP; Rossow & Schiffer, 1999) generally only observe radiation scattered or emitted from cloud top of optically thick clouds. Therefore, these satellites are generally not suitable for resolving the full vertical profile of clouds.

These issues are partially mitigated by active satellite instruments, such as the CloudSat Cloud Profiling Radar (CPR) (Stephens et al., 2008) and the Cloud-Aerosol Lidar with Orthogonal Polarization (CALIOP) instrument on the Cloud-Aerosol Lidar and Infrared Pathfinder Satellite Observations (CALIPSO) satellite (Winker et al., 2009). But even these instruments have limitations. For example, the CPR is affected by ground clutter below 1.2 km (Marchand et al., 2008) while the CALIOP lidar signal is attenuated by optically thick cloud. Given the high occurrence of low-level cloud in the Southern Ocean (Haynes et al., 2011), this factor has been studied to examine the level of underestimation (Alexander & Protat, 2018; McErlich et al., 2021). McErlich et al. (2021) compared two sets of satellite-derived cloud products, developed from a combination of CPR and CALIOP data, against ground-based observations made at the McMurdo station, Antarctica, collected during the Atmospheric Radiation Measurement West Antarctic Radiation Experiment (AWARE) campaign (Lubin et al., 2020). They highlighted that active satellite sensors underestimate low-level cloud relative to surface observations.

In particular, McErlich et al. (2021) showed that both the 2B-CLDCLASS-LIDAR R05 (2BCL5) (Sassen et al., 2008) and raDAR/liDAR (DARDAR) (Delanoe & Hogan, 2010) data products underestimate cloud occurrence below 1.5 km relative to surface observations, with both products distinguishing roughly one third of colocated cloud occurrences observed by AWARE at 0.5 km. Over the Arctic and the Antarctic, Silber et al. (2021) also found that differences in instrument sensitivity and detection algorithms can reduce spaceborne estimates of cloud and surface precipitation occurrence frequency by more than 50% relative to surface measurements. More widely, Liu et al. (2016) identified that the CPR experiences contamination in the lowest 1 km due to ground clutter that hinders detection of low marine clouds, inducing an underestimation of up to 39% over the oceans. Other parameters are also known to be affected by signal attenuation due to low-level clouds and ground clutter; for example, biases exist in satellite-based observations of radiation (Pei et al., 2023) when compared to Southern Ocean surface observations.

Surface and airborne observations over Antarctica and the Southern Ocean are thus of high value and provide a complement to satellite observations. But observational campaigns in the Southern Ocean (Kremser et al., 2021; McFarquhar et al., 2021; Sellegrí et al., 2023) and around Antarctica (Lubin et al., 2020; Scott & Lubin, 2014, 2016) are challenging, costly, and therefore rare (Lachlan-Cope, 2010). Surface observations of all types also have their own limitations. For example, the lidar signal from surface observations can be attenuated by optically thick low-level cloud which means that the occurrence of high-level clouds will be underestimated relative to satellite observations (McErlich et al., 2021). This can also influence integrated quantities, such as cloud fraction,

with Listowski et al. (2019) identifying that ceilometer observations of cloud fraction were significantly lower than corresponding values from the DARDAR product over Antarctica.

This study compares cloud data from a Vaisala CL51 ceilometer at Scott Base, Antarctica, with sets of data from three reanalyses after the application of an instrument simulator (Kuma et al., 2021). By simulating cloud properties which account for instrumental sensitivities, instrument simulators allow a direct quantitative comparison of cloud properties across diverse numerical models with observations which allows a like for like comparison. The use of instrument simulators alleviates some of the issues detailed in Silber et al. (2021). This analysis complements previous work in the region which has directly compared model output with observations. For example, a comparative analysis between observational data from McMurdo Station, Antarctica, and the Community Atmosphere Model version 6 (CAM6) simulations was detailed in Yip et al. (2021). They found that the CAM6 simulation consistently overestimates (underestimates) cloud occurrence above (below) 3 km in every season of the year. However, the effect of instrument sensitivities was not considered in that work. Previous work detailed in Kuma et al. (2020) compared ceilometer observations collected across a set of 5 voyages in the Southern Ocean against nudged output from the Global Atmosphere (GA) version 7.1 of the HadGEM3 GCM and MERRA2 reanalysis output processed using an instrument simulator. Notably, they found that both the GA7.1 and MERRA2 underestimate low cloud and fog occurrence relative to the ship observations by 4%–9% for GA 7.1% and 18% for MERRA2.

A number of studies have previously attempted to quantify the quality of reanalyses products around Antarctica (Bracegirdle, 2013; Bracegirdle & Marshall, 2012; Fogt et al., 2017; McDonald & Cairns, 2020; Nygard et al., 2016; Reid et al., 2024; Schneider & Fogt, 2018). Studies have identified spurious trends in reanalyses in the temperature (Huai et al., 2019), pressure (Schneider & Fogt, 2018), precipitation (Reid et al., 2024), and surface wind (Nygard et al., 2016) fields around the Antarctic continent. More specifically, work in Coggins et al. (2014) compared wind speeds from ERA-Interim and automated weather station winds over the Ross Sea and Ross Ice Shelf and found ERA-interim underestimated wind speeds during strong wind events. Work in Dale et al. (2017) also found a similar result at the front of the Ross Ice Shelf close to the Ross Sea polynya region. More recent work by McDonald and Cairns (2020) identified that the surface wind patterns over the Ross Sea derived by the ERA5, ERA-Interim, JRA55, and MERRA2 reanalyses are highly consistent over the satellite era. While not over the Antarctic continent, comparisons detailed in McErlich et al. (2023) between ERA5 reanalyses and WindSat satellite observations identify that ERA5 underestimates total column water vapor and surface wind speeds by a few percent. Notably, cloud liquid water is underestimated by up to 40% near cyclone centers. ERA5 also underestimates precipitation in the warm sector of cyclones by up to 15%, but overestimates it in the cold sector by up to 60%. However, to our knowledge this is the first study to complete a critical analysis of the representation of clouds relative to multiple reanalyses products in Antarctica, and therefore broadens our knowledge of the quality of these products.

## 2. Data and Methodology

Observations from a Vaisala CL51 ceilometer operating at a wavelength of 910 nm (near infrared) deployed at Scott Base (77.8°S, 166.7°E) between February 2022 and December 2023 are used in this study. This wavelength is characterized by relatively low molecular backscattering, but is affected by water vapor absorption (Wiegner & Gasteiger, 2015). The maximum range of the instrument is 15.4 km, with a sampling rate of 6 s and a vertical resolution of 25 m. This instrument produces data files containing uncalibrated attenuated volume backscatter coefficients which are converted to NetCDF using the cl2nc software (Kuma, 2020). These NetCDF files are then processed with the Automatic Lidar Ceilometer Framework software (Kuma et al., 2021) detailed in Section 2.1.

The present study uses outputs from three reanalyses, ECMWF Reanalysis 5 (ERA5) (Hersbach et al., 2020), Japanese 55-year Reanalysis (JRA55) (Kobayashi et al., 2015) and Modern-Era Retrospective analysis for Research and Applications, version 2 (MERRA2) (Gelaro et al., 2017). ERA5 is the fifth-generation ECMWF reanalysis model (Hersbach et al., 2020). The cloud and precipitation properties (i.e., cloud fraction, cloud ice, cloud liquid, rain, and snow water content) in ERA5 are prognostically estimated based on Tiedtke (1993), which considers physical processes as sources or sinks. Additionally, the prognostic scheme detailed in Forbes and Ahlgren (2014) represents the phase partitioning in mixed-phase clouds.

We also use the Japanese 55-year Reanalysis (JRA55); this reanalysis extends for a 55-year period starting from 1958, when regular radiosonde observations became operational globally. Details about JRA55 are detailed in

Kobayashi et al. (2015). Clouds and their water content in JRA55 are prognostically derived from the probability density function of the total water content using the scheme detailed in Smith (1990). Cloud fractions are derived where the total water content in a grid box exceeds the saturation specific humidity. For marine stratocumulus clouds, cloud fraction is derived diagnostically using the vertical gradient of the potential temperature (Kawai & Inoue, 2006).

This study also uses data from the Modern-Era Retrospective analysis for Research and Applications (MERRA2) reanalysis (Gelaro et al., 2017). We used the 3-hourly instantaneous assimilated meteorological fields (`inst3_3d_asm_Nv` (`M2I3NVASM`)), to generate simulated ceilometer profiles using Automatic Lidar and Ceilometer Framework (ALCF). The four-dimensional MERRA2 fields were provided on pressure and model levels. MERRA2 uses a prognostic scheme for simulating nonconvective clouds, including condensation, autoconversion, and evaporation (Bacmeister et al., 2006). Cloud fraction and condensate in MERRA2 are estimated by integrating the probability density function of total water within each grid box over regions that exceed a critical relative humidity threshold. The analyzed time period of all three reanalyses data sets was between 14 February 2022 and 31 December 2023 unless otherwise stated. The three reanalyses data sets also have different horizontal resolutions with ERA5 having  $0.25 \times 0.25^\circ$ , MERRA2 having  $0.625 \times 0.5^\circ$ , and JRA55 having  $1.25 \times 1.25^\circ$  longitude-latitude grids.

As previously identified to our knowledge, no study examining the quality of multiple reanalyses cloud representation has occurred over Antarctica. The present study aims to fill this gap by comparing reanalyses output with ceilometer data. Ceilometers can provide valuable information on cloud and aerosols, but have not been widely used in the evaluation of climate models, reanalyses, or numerical weather prediction models. This is partially related to the wide range of ceilometer instruments, a lack of standardized calibration, and the difficulty in directly comparing observations with model outputs. The ALCF software allows the calibration of ceilometer data and its instrument simulator reduces uncertainty when comparing observations with model output.

## 2.1. ALCF

This study uses the ALCF tool which was first used in Kuma et al. (2020) and was subsequently described in more detail in Kuma et al. (2021). ALCF provides a framework for converting ceilometer data from different manufacturers into a common format, calibrates the backscatter data, resamples data, and also completes a noise removal and cloud detection process.

ALCF also includes a ground-based lidar simulator, which calculates the radiative transfer of laser radiation and allows one-to-one comparison between models and observations. The ALCF ground-based lidar simulator is a development of the CFMIP Observation Simulator Package (COSP) (Bodas-Salcedo et al., 2011), a set of instrument simulators developed by the Cloud Feedback Model Intercomparison Project. COSP was originally developed as a satellite simulator package whose aim is to produce virtual satellite (and more recently ground-based) observations from atmospheric model fields in order to improve comparisons of model output with observations (Bodas-Salcedo et al., 2011). This approach is required because physical quantities derived from satellite observations generally do not directly correspond to model fields. ALCF developed a ground-based lidar simulator by modifying the COSP Active Remote Sensing Simulator (Chiriacò et al., 2006). This extension produces virtual backscatter measurements from model fields. Resampling, noise reduction, and cloud detection were also performed on observational and derived model lidar output in a consistent way to reduce structural uncertainty. ALCF developments required reversing the vertical layers, as the surface lidar looks from the surface up rather than down from space to the surface, and changing the radiation wavelength affecting Mie scattering by cloud droplets and Rayleigh scattering by air molecules. We only present a brief description of the surface lidar simulator and instead encourage interested readers to examine Kuma et al. (2021).

The recently introduced COSP version 2 (Swales et al., 2018) added support for a surface lidar simulator, although we believe that ALCF, developed before COSPv2 was available, is more complete in the present context due to its treatment of Mie scattering at wavelengths other than 532 nm (the wavelength of the CALIOP lidar). It also adds a more detailed simulation of ice crystal optical properties. The surface lidar simulator takes model cloud liquid and ice mixing ratios, cloud fraction, and thermodynamic profiles as the input, and calculates vertical profiles of attenuated backscatter. We also note that we used the ALCF software to create calibration coefficients for the CL51 ceilometer using the methodology detailed in O'Connor et al. (2004) rather than using the default CL51 calibration available within the package.

## 2.2. Supercooled Cloud Detection

Guyot et al. (2022) developed an algorithm to detect supercooled liquid water containing clouds (SLCC) based on the copolarization backscatter measured by ceilometers using observations from a training data set collected at the Davis station, Antarctica. This classification model used an extreme gradient boosting (XGBoost) framework ingesting backscatter data with an accuracy as high as 91%. More recently, the same framework has also been applied with modifications over midlatitudes by Whitehead et al. (2024), the modifications being necessary because regions which also include warm liquid cloud impact the accuracy of the Guyot et al. (2022) scheme outside the polar environment. This study applies the Guyot et al. (2022) classification scheme to ceilometer backscatter measurements made at Scott Base. We note that a validation of the Guyot et al. (2022) scheme is not possible without reference data. But visual inspection initially identified poor classification results when the Guyot et al. (2022) scheme was applied to Scott Base data using the default ALCF calibration coefficient for a CL51 ceilometer. However, after using the O'Connor et al. (2004) methodology to calibrate the ceilometer, the scheme worked well based on visual inspection, with perhaps some periods where SLCC is underreported. We thus detail the results of the application of the Guyot et al. (2022) classification scheme to the CL51 backscatter data in this paper.

## 2.3. Weather Typing

Jolly et al. (2018) suggested that cloud occurrence over the Ross Ice Shelf is strongly impacted by synoptic state, and this variation is significantly larger than the observed seasonal cycle. We therefore create a set of weather states using a similar methodology to that used in McDonald and Cairns (2020). In particular, our weather types are derived using the self-organizing map (SOM) technique applied to ERA5 10-m wind speeds between 1979 and 2023 to derive representative surface wind patterns. However, in this case we found that our results were sensitive to the geographical domain used; we therefore use a more local domain between latitudes of 75° and 80°S and longitudes from 150° to 185°E in the analysis presented. This suggests that the local flow around Ross Island and Minna Bluff to the south strongly influence the cloud environment at Scott Base.

SOMs are an iterative unsupervised learning scheme commonly used in clustering (Kohonen, 1990). The learning process adjusts a set of reference vectors based on the differences between the reference vector and each input record. A learning rate determines how the adjustment is related to the difference between the reference vector and the input data measured by the Euclidean distance metric. Training then entails adjusting reference vectors iteratively until a set of stable values are reached. The learning rate and width of the kernel are reduced as a function of time such that the SOM evolves rapidly initially. The Euclidean distance is used to identify reference vectors within a certain range of the best matching vector. The vectors that fall within this neighborhood are then updated which produces the coherent organization of output. During each iteration, the reference vector that best matches the input record is identified and then modified to better reflect the input data. The training process ultimately produces reference vectors that represent the multidimensional input space.

Rather than applying the SOM technique directly to all the ERA5 output, we reduce the quantity of input into the SOM by applying an empirical orthogonal function analysis to the space-time cube of the surface winds (both zonal and meridional winds) and then apply the SOM technique to the largest principal components (PCs) only. In this study, we truncated the set of PCs when the explained variance was 90% of the total variance of the data set. In this study, we used the implementation of the SOM methodology available in the mini-SOM python package (Vettigli, 2018).

The usage of the empirical orthogonal function analysis requires anomalies as inputs and the climatological mean from each latitude/longitude point for the 1979–2023 reference period was used to derive these anomalies. Our analysis focuses on the geographic domain (60–90°S, 140–220°E) used previously in McDonald and Cairns (2020). We also derived a daily average to reduce the processing requirements for the study. Previous work detailed in Tastula et al. (2013) identified that near-surface wind speed displays low diurnal variability in both observations and in reanalyses products over Antarctica, and thus, our choice to use daily averages should not impact our results.

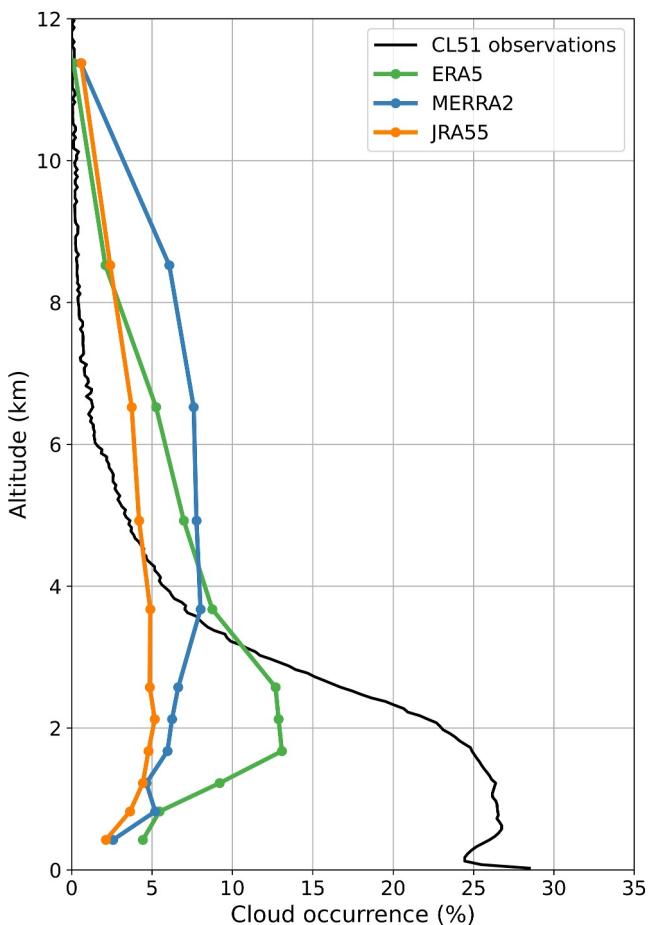


**Figure 1.** Mean vertical profiles of cloud occurrence for the period from 14 February 2022 to 31 December 2023 derived from CL51 ceilometer observations (black line) and the ERA5 (green line), JRA55 (orange line), and MERRA2 (blue line) model fields after processing using the Automatic Lidar and Ceilometer Framework ground-based lidar simulator.

cloud occurrence will be underestimated (McErlich et al., 2021). This comparison highlights the importance of different instrument sensitivities. Comparison between model properties and observations which do not account for instrument sensitivities can thus bias model evaluations.

Comparison between the CL51 observations and the ERA5, JRA55, and MERRA2 cloud occurrence profiles derived using ALCF displayed in Figure 1 show low-biased values relative to the CL51 observations of cloud occurrence for altitudes below 3 km and high-biased cloud occurrences in ERA5, JRA55, and MERRA2 above that altitude.

Work detailed in Yip et al. (2021) compared the same AWARE observations as used in Silber et al. (2018) with CAM6 model data. The CAM6 simulations examined in Yip et al. (2021) were nudged toward MERRA2 reanalyses temperature and wind fields. Similar to our results, they identified sizable overestimates (underestimates) of cloud occurrence above (below) 3 km in the model. We also note that the general form of the vertical profile of cloud occurrence in MERRA2 displayed in Figure 1 is rather similar to the CAM6 equivalent, though the CAM6 cloud occurrence is roughly 15% greater than the corresponding MERRA2 values at the same altitude. This is likely associated with changes in the comparison process due to the use of an instrument simulator in this study.

Yip et al. (2021) also identified that cloud occurrence biases were closely associated with concurrent biases in relative humidity in the CAM6 model with high relative humidity biases between the CAM6 data and observations above 2 km and low relative humidity biases below 2 km. To test whether this may also be a controlling factor for the three reanalyses, we compare the relative humidity from the reanalyses with radiosonde

### 3. Results

Figure 1 displays the mean cloud occurrence as a function of altitude derived from the CL51 ceilometer observations, and predictions of cloud occurrence derived using the ALCF surface lidar simulator from input from ERA5, JRA55, and MERRA2 models. These mean values are derived for the period from 14 February 2022 to 31 December 2023 where both ceilometer and model outputs are available. The maximum cloud occurrence for the CL51 observations peaks at the surface, but this peak is potentially contaminated by low-level fog and wind blown snow below the commonly observed low-level inversion layer (Hofer et al., 2021). The backscatter near the surface is also more uncertain because of the overlap function used. Thus, the secondary peak with a value of just over 25% cloud occurrence at approximately 800 m above the surface is likely the true maxima observed by this system. These values of cloud occurrence at this peak are roughly 10% lower than previous surface observations from the McMurdo station detailed in Silber et al. (2018). Though the general form of the vertical profile of cloud occurrence is very similar. The difference may be partially connected to the greater attenuation of the ceilometer signal due to obscuring optically thick clouds compared to those detailed in Silber et al. (2018) which used a more powerful lidar instrument and also included information from a Ka-band cloud radar. The high spectral resolution lidar (HSRL) is also more sensitive to tenuous cloud. Additionally, the variability from day-to-day, seasonally and with synoptic types is large based on the ground-based observations discussed in Silber et al. (2018) and therefore interannual variability could also partially explain this difference. We also note that the cloud thresholding scheme available in the ALCF software likely provides a conservative estimate of cloud occurrence.

Satellite observations averaged over the Ross Ice Shelf detailed in Jolly et al. (2018) show peak cloud occurrences between 20% and 30% at approximately 2 km for all seasons which are larger than the peak values observed by the CL51 ceilometer in Figure 1. However, the satellite observations have lower cloud occurrences than the CL51 ceilometer values at altitudes below approximately 2 km. This difference is likely due to different instrument sensitivities. In particular, satellite observations of low-level cloud will likely be underestimates, while ground-based observations of upper-level

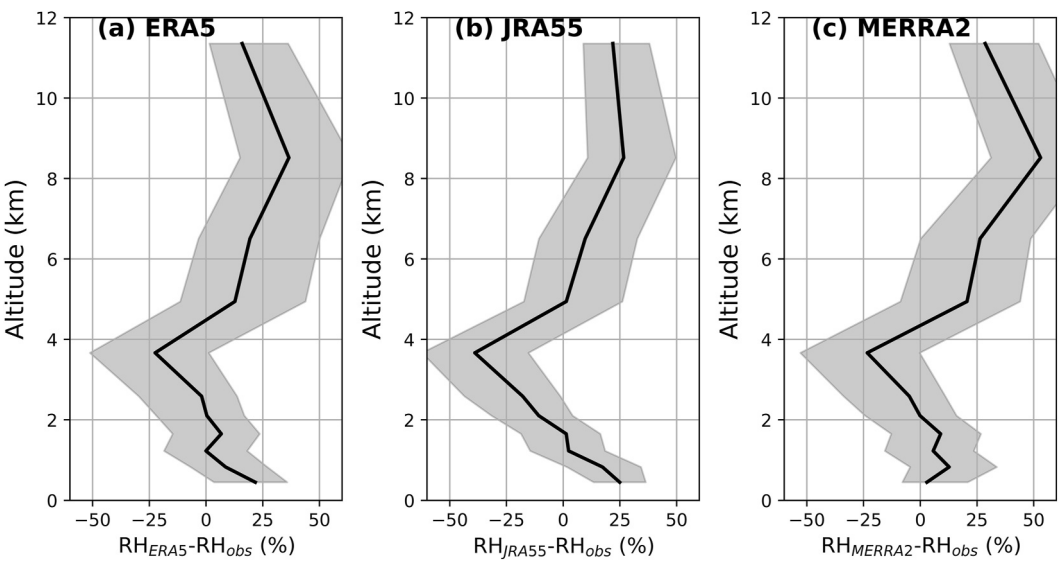


**Figure 2.** Median and interquartile ranges of the difference between radiosonde observations and reanalyses values of relative humidity for the (a) ERA5, (b) JRA55, and (c) MERRA2 reanalyses.

observations launched from the nearby (less than 3-km separation) McMurdo station. Figure 2 displays the median and interquartile ranges of the difference between radiosonde observations and the three reanalyses (model-observation). The difference between the McMurdo radiosonde relative humidity and the ERA5 values, shown in Figure 2a, display overestimates of the relative humidity below 2 km, a region of underestimates between 2 and 4.5 km and larger overestimates above this altitude. A similar pattern of bias between the observations and the JRA55 reanalyses relative humidity is displayed in Figure 2b, though the biases are larger than those from the ERA5 data set apart from at around 9 km. The MERRA2 observations display the same structure of bias as ERA5 and JRA55 relative to the radiosonde observations. We note that the biases identified are larger than might be expected given that radiosonde data are routinely assimilated into all three reanalyses. However, Jung et al. (2016) identifies that the combination of sparse observations and a lack of optimization of data assimilation methods for high latitudes limit the quality of reanalyses in these regions potentially explaining this issue.

Figures 3a–3d displays vertical profiles of the median and interquartile range cloud occurrence for each season from the ceilometer observations and the three reanalyses. Examination of the CL51 observations shows the largest cloud occurrences and the largest range of values occurs in austral autumn (MAM) and winter (JJA) and smaller cloud occurrences and interquartile ranges in austral spring (SON) and summer (DJF). In particular, the median cloud occurrence is up to 25% in austral autumn and winter, but below 20% in austral spring and summer. However, in every season, the largest cloud occurrences are observed in the 2 km directly above the surface in the CL51 observations, and cloud occurrence reduces relatively quickly between 2 and 4 km to only a few percent above 4 km in all seasons. The reanalyses' results display marginally higher values in austral spring, but small seasonal variations. It is also relatively clear that cloud occurrences are lower in the JRA55 reanalysis than the other two reanalyses which show more comparable results. Though, as previously seen in Figure 1, the MERRA2 model output has higher cloud occurrences at higher altitudes than the ERA5 values.

The biases between the reanalyses and the CL51 ceilometer observations (model observations) are shown in Figures 3e–3h for each season. In each season, a large underestimate (15%–30%) in cloud occurrence is observed for all three reanalyses below 3 km with a smaller overestimate in cloud occurrence in the reanalyses above 3 km. Interestingly, the bias at low altitudes is comparable to the values identified by Yip et al. (2021) and Kuma et al. (2021). The ERA5 reanalysis displays the smallest biases of the three reanalyses at most altitudes in most seasons. The JRA55 reanalysis displays the largest underestimates below 3 km in all seasons, and the MERRA2 reanalysis has the largest overestimates relative to the CL51 observations above 3 km in all seasons. Closer inspection of Figures 3e–3h shows variations in the bias with season, with the largest underestimates below 3 km in austral autumn and winter and the smallest underestimates in austral spring and summer. An examination of the altitudes where the reanalyses overestimate cloud occurrence also shows that the austral spring displays the

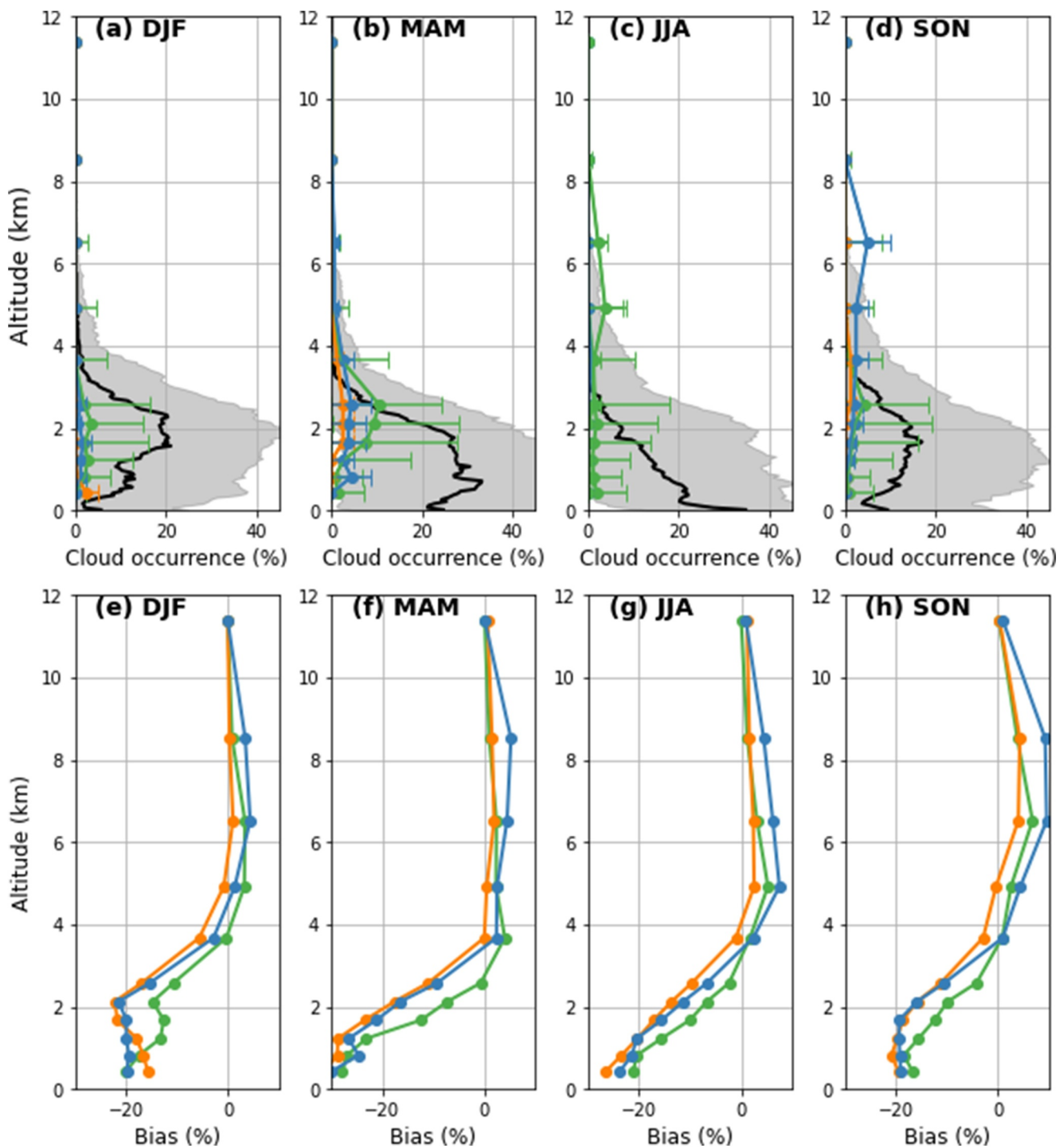


**Figure 3.** Median and interquartile ranges of cloud occurrence vertical profiles derived from CL51 ceilometer observations (black line), and ERA5 (green line), JRA55 (orange line), and MERRA2 (blue line) model fields after processing using the Automatic Lidar and Ceilometer Framework ground-based lidar simulator are displayed for (a) austral summer, (b) autumn, (c) winter, and (d) spring. The model bias (model minus observation means) is also shown for (e) austral summer, (f) autumn, (g) winter, and (h) spring.

largest overestimates, which reach 10% in MERRA2. Notably, the magnitudes of the underestimated and overestimated values are more similar in Yip et al. (2021) than in this study. This difference can likely be explained by the use of an instrument simulator in this study which allows a more robust comparison between the

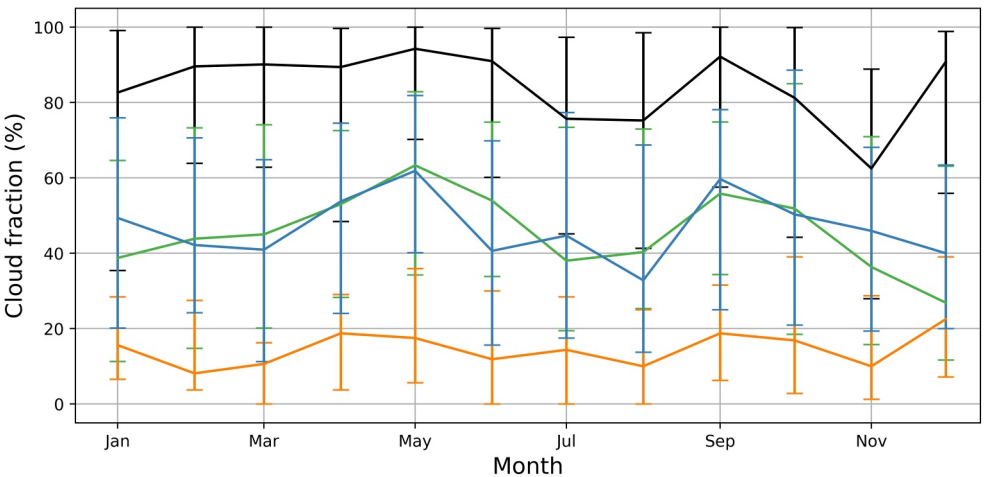


**Figure 4.** Median and interquartile ranges of cloud fraction each month derived from CL51 ceilometer observations (black line), and ERA5 (green line), JRA55 (orange line), and MERRA2 (blue line) model fields after processing using the Automatic Lidar and Ceilometer Framework ground-based lidar simulator.

observations and the model output. Effectively, the low cloud occurrences in the observations at higher altitudes are likely impacted by instrument sensitivity which means that they are likely low-biased estimates.

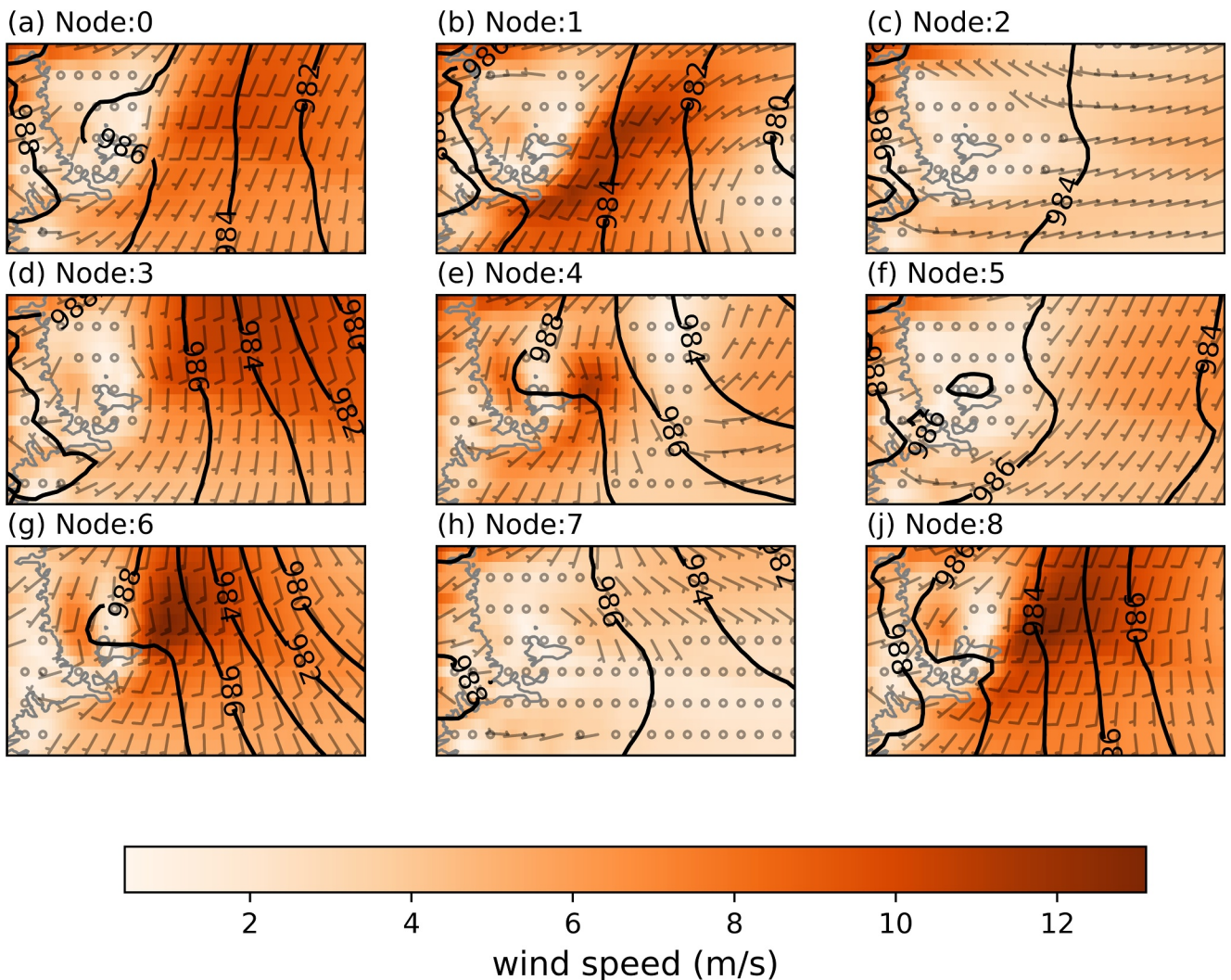
The median and interquartile ranges for cloud fraction, which is defined in this study as the integrated cloud occurrence over all altitudes at each time step, averaged for each month are displayed in Figure 4. A quite small variation in the median cloud fraction between months is observed for both the CL51 observations and the three reanalyses. In particular, for the CL51 observations and for the three reanalyses, the interquartile range in any month usually contains the range of median values for all months. However, comparison of the median cloud fraction between the CL51 observations and the three reanalyses very clearly shows large offsets. In particular, the median values of cloud fraction for the CL51 observations are between 62% and 92%, the ERA5 values are between 27% and 63%, the JRA55 values are between 10% and 22%, and the MERRA2 values are 32%–62%. It is thus very clear that all three reanalyses underestimate cloud fraction, though the underestimate is particularly large for the JRA55 reanalyses.

### 3.1. Weather Classification

The relatively small variation between the different seasons observed in Figures 3 and 4 has previously been identified in other studies. In particular, Jolly et al. (2018) and Silber et al. (2018) identified that the synoptic situation has a much larger impact on vertical cloud distributions in this region than seasonal variability. We therefore complete a weather classification over the local Ross Sea region; this allows the CL51 ceilometer data collected from Scott Base between February 2022 and January 2024 to be categorized based on weather state. The method used to complete this weather classification is detailed in Section 2.3. The surface horizontal wind vectors and wind speeds associated with each weather state are shown in Figure 5 over the Ross Island region. This classification is used to group the corresponding data from the CL51 observations and the output of the ALCF lidar simulator derived from the three reanalyses in Figure 6.

A  $3 \times 3$  SOM (3 columns and 3 rows) was selected for our classification because it minimized quantization error and represented a good balance in terms of representation of the wind patterns over the region. The set of nodes from this reference period is used throughout this study for grouping the ceilometer data collected and also to group the corresponding data from the ALCF lidar simulator (Kuma et al., 2021) derived from the ERA5, JRA55, and MERRA2 models.

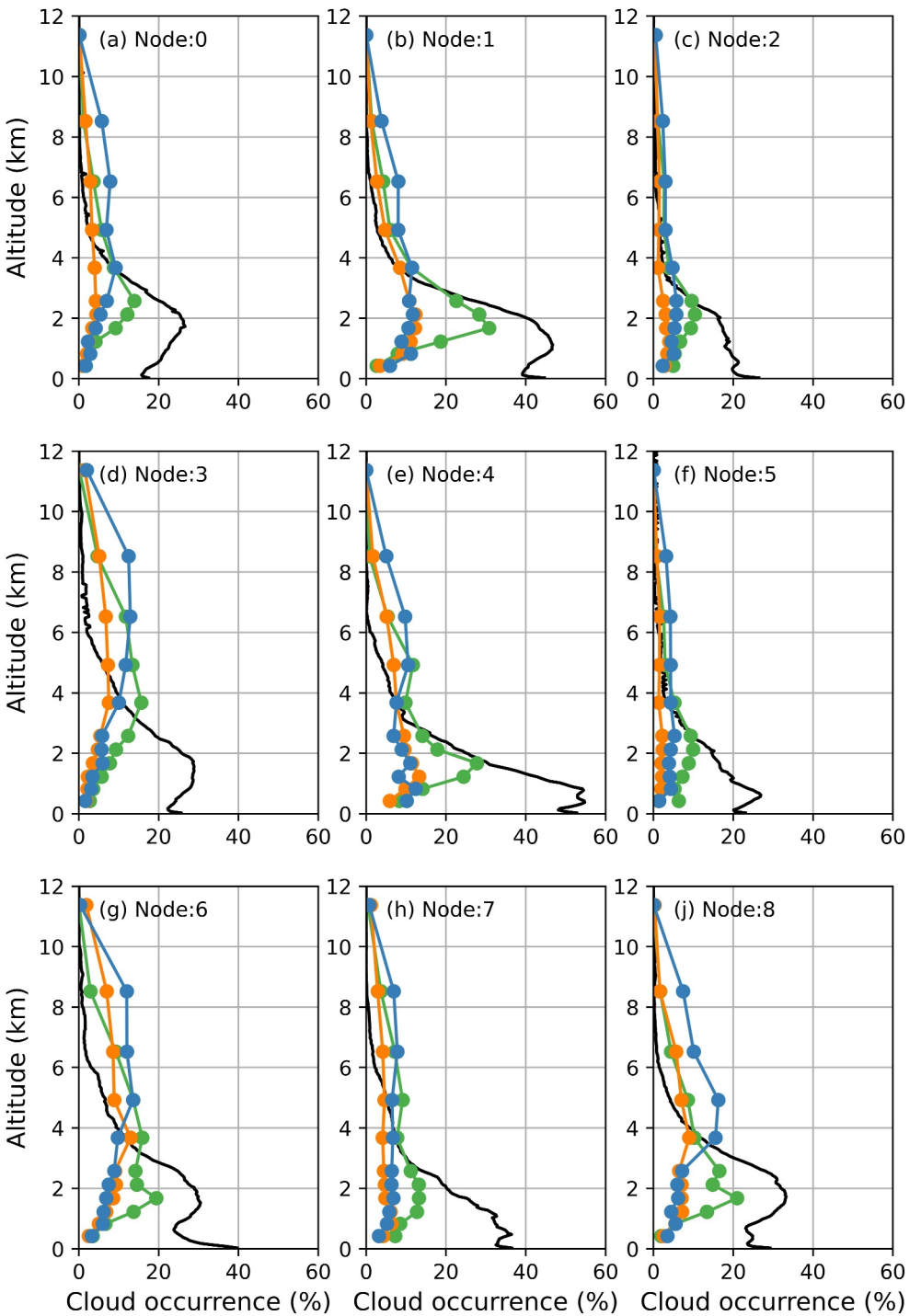
The different wind patterns in Figure 5 are dominated by southerly winds in all of the nodes derived, except for node 2. But the magnitude of the wind changes significantly. For example, nodes 2 and 5 display weak winds directly over Ross Island, the site of Scott Base and the ceilometer, while node 1 displays rather strong winds directly to the east of Ross Island. We also note that the nodes at the opposite corners of the SOM (node 2 and 6) display the largest difference in terms of wind magnitudes. Node 2 is also dominated by westerly winds. The



**Figure 5.** Near-surface (10 m) horizontal wind speeds and directions for each of the nine nodes in the self-organizing map derived from ERA5 reanalysis output for the period 1980–2024. The black contours identify corresponding isobars in hPa.

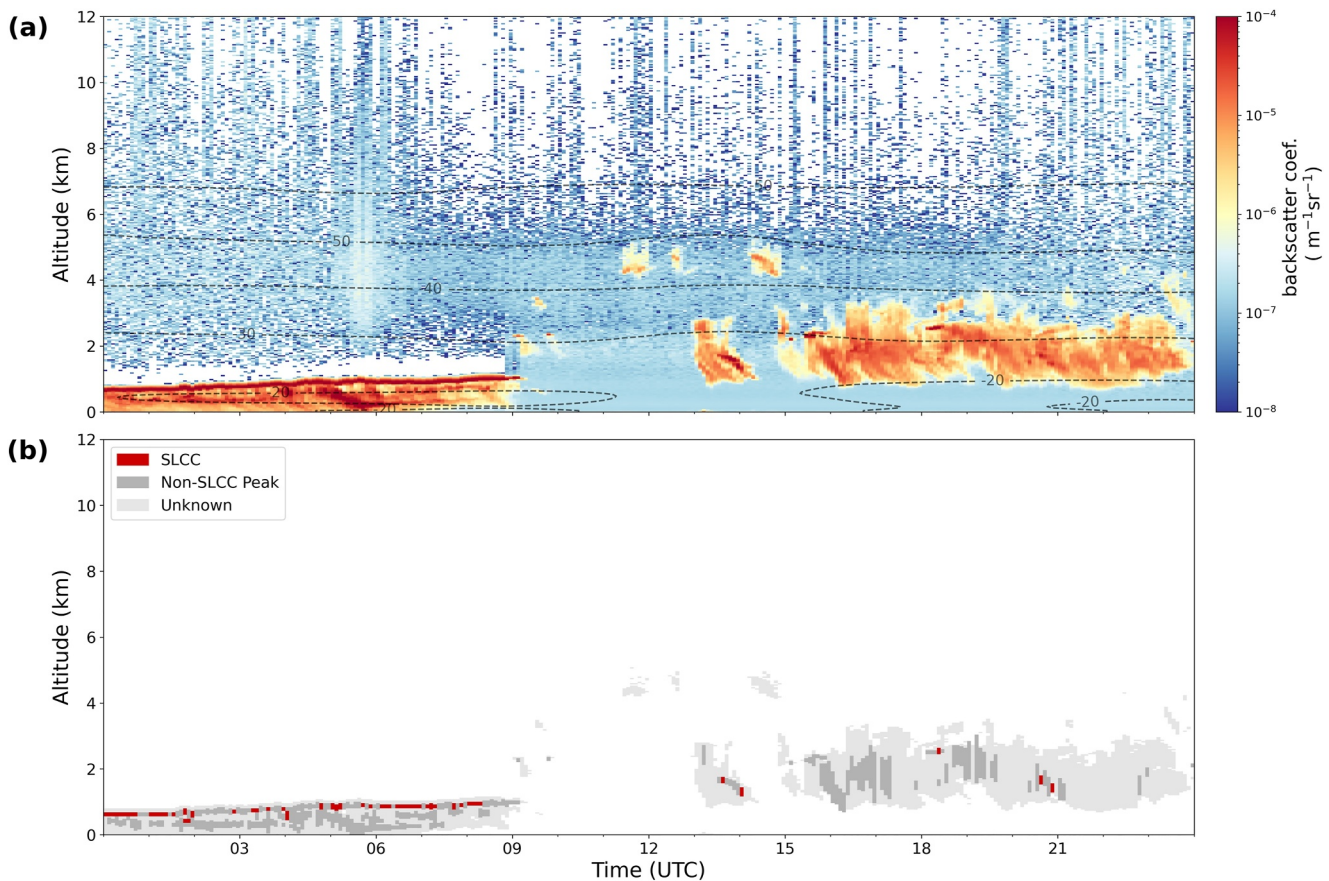
patterns identified in the various nodes are all strongly affected by the exact position of low pressure systems, with Node 3, 4, and 6 displaying a low pressure system to the northeast, while Node 1 and 8 have low pressure systems more directly east. This pattern aligns well with existing classifications in this region detailed in Coggins et al. (2014) and Seefeldt and Cassano (2008) which show that the region is often dominated by a low pressure to the east and isobars that align approximately with the topography of the Transantarctic Mountains. When this pressure gradient is strong and near perpendicular to the Transantarctic Mountains, a low-level barrier wind called the Ross Ice Shelf air stream is produced. We hypothesize that the importance of the local winds in this study is associated with how air is directed toward the high mountains that make up Ross Island, with Mount Erebus directly north of Scott Base.

Figure 6 displays vertical profiles of cloud occurrence for the CL51 observations and the results of the application of the ALCF instrument simulator to the three reanalyses grouped based on the weather conditions displayed in Figure 5. Examination of the CL51 cloud occurrence patterns shows significantly larger variability between weather states (Figure 6) than for different seasons (Figure 3). In particular, nodes 1 and 4 display maximum cloud occurrences above 40% at altitudes below 2 km though the cloud occurrence begins to fall from around 50% from 1 km while the lowest CL51 cloud occurrences are observed in node 2 and 5. We also note that high cloud occurrences are very close to the surface in nodes 6 and 7 which potentially suggests the presence of wind-blown snow, fog, or low-level temperature inversions in these local weather situations.



**Figure 6.** Mean vertical profiles of cloud occurrence for each weather state for CL51 ceilometer observations (black), and ERA5 (green), JRA5 (orange), and MERRA2 (blue) model fields.

Vertical profiles of the cloud occurrence derived from the ERA5 reanalysis show higher values for node 1 and 4 close to 2 km and lower values in node 2 and 5 in Figure 6. These patterns match closely with the CL51 ceilometer observations for these weather situations above 2 km. However, the cloud occurrence is underestimated for all nodes below 2 km. Additionally, nodes 6, 7, and 8 display substantial overestimates in a relative sense for cloud occurrence above 2 km.



**Figure 7.** CL51 ceilometer-attenuated volume backscatter coefficient data over (a), and the Guyot et al. (2022) cloud mask (b) for 27 March 2022. AMPS air temperature contours are overlaid in (a) for reference.

Vertical profiles of the cloud occurrence derived from the JRA55 and MERRA2 reanalyses also show higher values for node 1 and 4 and lower values in node 2 and 5 in Figure 6. However, these patterns match much less closely with the CL51 ceilometer observations than the ERA5 values. The patterns are quite consistent between the JRA55 and MERRA2 simulation results, though notably, the MERRA2 cloud occurrences are higher at nearly every altitude in every node than the corresponding JRA55 values. Additionally, for nodes 3, 6, 7, and 8 the JRA55 and MERRA2 values display substantially overestimated cloud occurrence above 2 km relative to the CL51 ceilometer observations. These overestimates are also significantly larger than those observed between ERA5 and the CL51 ceilometer observations. However, the cloud occurrence is underestimated for all nodes below 2 km.

### 3.2. Cloud Phase Analysis

To obtain more information from the ceilometer observations, we apply the XGBoost algorithm detailed in Guyot et al. (2022) to derive the fraction of cloud that is associated with supercooled liquid water. Figure 7a displays the attenuated volume backscatter coefficient data over Scott Base for 27 March 2022. On this day, a narrow band of low-altitude ( $< 1 \text{ km}$ ) multilayer cloud occurs between 00:00 and 09:00 UTC, while a thicker band of cloud is present at altitudes ranging from 1 to 3 km between 15:00 and 23:00 UTC. The cloud classification displayed in Figure 7 displays thin ice cloud layers close to the surface between 00:00 and 09:00 UTC capped by strongly attenuating supercooled cloud layers. The thicker cloud layer between 15:00 and 23:00 UTC either has an ice cloud or undefined classification. The presence of a small amount of supercooled liquid cloud within that thicker layer may suggest the presence of mixed-phase cloud or may be a classification error. The lack of depolarization data from the CL51 ceilometer means that we cannot validate the Guyot et al. (2022) scheme. But visual inspection does suggest that the strongly attenuating cloud layer between 00:00 and 09:00 UTC is correctly

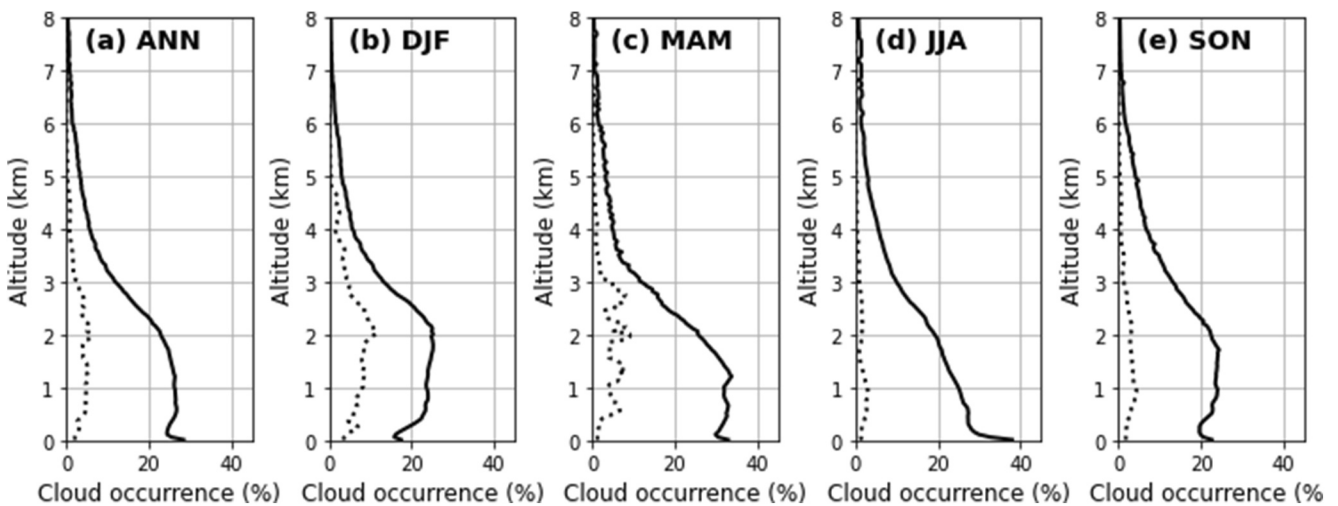


**Figure 8.** (a) Mean vertical profiles of cloud occurrence averaged over the observational period and (b) austral summer, (c) spring, (d) winter, and (e) autumn derived from CL51 ceilometer observations (black line) and the corresponding supercooled liquid water occurrence (black dotted line).

classified as supercooled liquid cloud. Though the lack of continuity in the backscatter coefficient data for that layer suggests that any estimates of supercooled liquid water cloud presence are likely to be conservative. This also tallies with results from Guyot et al. (2022) which came to the same conclusion. We also note the relatively high proportion of undefined clouds in this case, which means that these peaks in the attenuated volume backscatter coefficient cannot be classified as either ice or supercooled liquid water. This is potentially due to the presence of mixed-phase cloud in our observations. We also reiterate that the classification scheme detailed in Guyot et al. (2022) does appear to be sensitive to the calibration factors applied to the data. We thus advise future users to complete calibration using the O'Connor et al. (2004) or Hopkin et al. (2019) scheme rather than using default values from ALCF.

The application of the Guyot et al. (2022) XGBoost scheme allows us to derive the fraction of cloud peaks classified as supercooled liquid water relative to other classes (the combination of ice and undefined). The mean fraction of supercooled liquid water cloud as a function of altitude can then be derived from the CL51 ceilometer observations between 14 February 2022 and 31 December 2023. Figure 8a displays vertical profiles of the occurrence of supercooled liquid water cloud and all clouds. We note that the supercooled liquid water cloud occurrence remains relatively constant between 0.5 and 2.5 km at 5%, and then rapidly declines to near-zero values above 4 km. The form of this vertical profile is very similar to that previously displayed in Silber et al. (2018) with near constant values between 0.5 and 3 km, though we note that the cloud occurrence is again lower than that identified. We again believe that this is associated with differences in the capability of the HSRL used in Silber et al. (2018) and the CL51 ceilometer observations used in the present study.

Figures 8b–8e display the mean cloud occurrence and the supercooled liquid water cloud fraction for each season. The mean cloud occurrence displays similar patterns to the median values previously shown in Figure 3 as expected. Comparison of the supercooled liquid water cloud occurrences between the seasons shows the highest supercooled liquid water fractions in austral summer (Figure 8b) and the lowest values in the austral winter (Figure 8d). Thus, while the vertical profile of cloud occurrence is strongly defined by weather state (see Figure 6), the cloud phase is strongly controlled by season. This likely reflects variations in the occurrence of temperatures between the 0°C isotherm and the homogeneous freezing level ( $-38^{\circ}\text{C}$ ) with season. At this point, we reiterate that the XGBoost classification includes a relatively high proportion of unclassified cloud, so that these results likely represent a conservative estimate of the fraction of supercooled liquid water and cannot be used to identify that all the rest of the cloud is glaciated.

The Guyot et al. (2022) XGBoost scheme requires information on the width of cloud peaks. In particular, supercooled liquid water cloud is partially identified by narrow peaks in the vertical profiles of the attenuated volume backscatter coefficient. The low vertical resolution of the reanalysis and its varying vertical resolution with altitude precludes the use of the scheme as derived in Guyot et al. (2022) on this model output. Further work

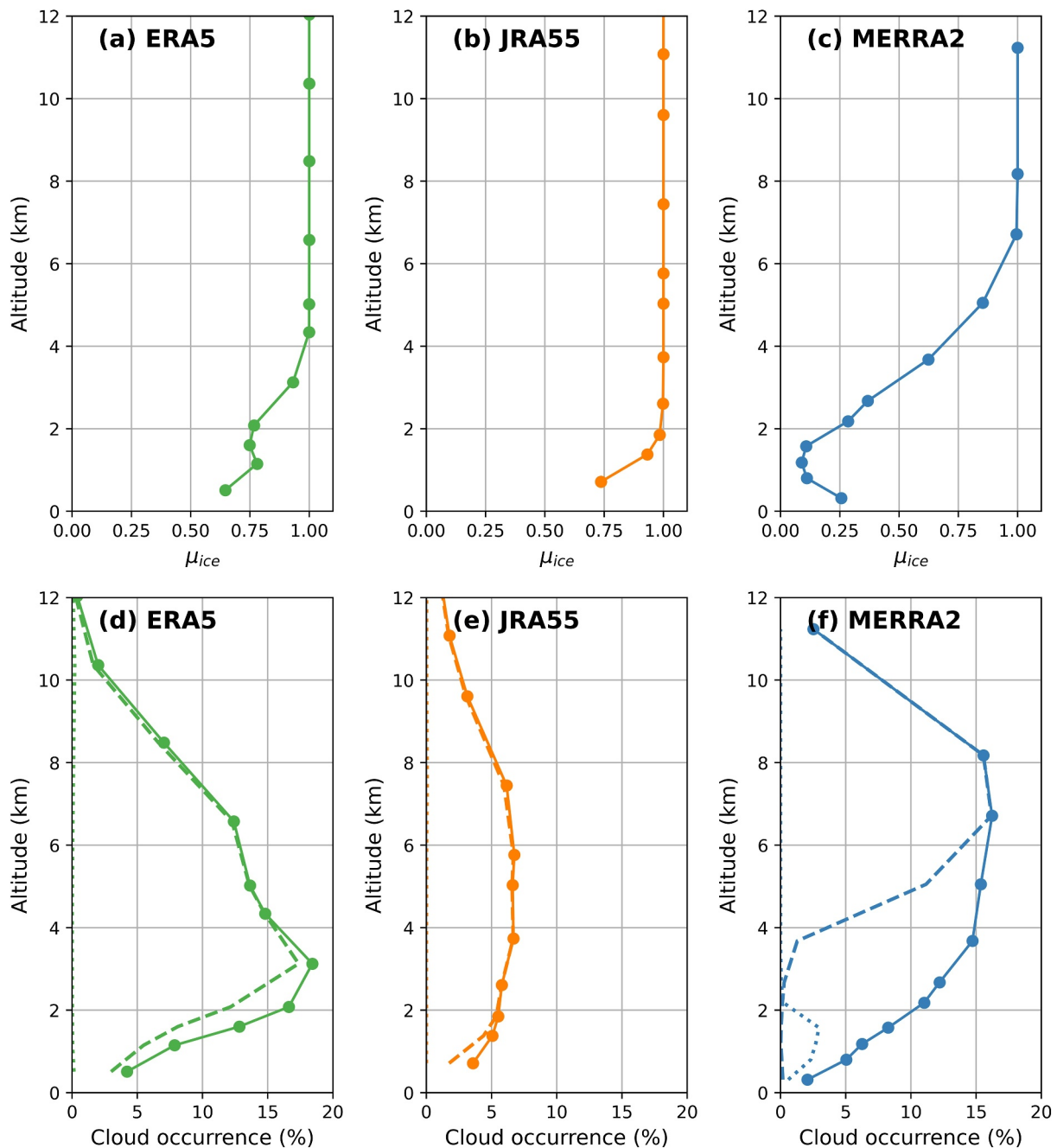


**Figure 9.** Mean vertical profiles of the ice water fraction ( $\mu_{ice}$ ) for the (a) ERA5, (b) JRA55, and (c) MERRA2 reanalysis. Mean vertical profiles of the cloud occurrence (full line) from the (d) ERA5, (e) JRA55, and (f) MERRA2 reanalysis. The cloud occurrence associated with ice (dashed line) and liquid (dotted line) water derived from the analysis of  $\mu_{ice}$  using the methodology detailed in Desai et al. (2023), as well as the total cloud occurrence (full line) are presented in (d) through (f). Note that cloud occurrences has not been derived from data processed using the Automatic Lidar and Ceilometer Framework lidar simulator.

could apply the XGBoost scheme without including a peak width input to rectify this issue, but this is outside the scope of the present work. Instead, we apply the simple scheme detailed in Desai et al. (2023) in which the cloud phase is defined using the ice mass fraction ( $\mu_{ice}$ ). The ice mass fraction is shown in Equation 1 and is obtained by taking the ratio of the ice water content to the total water content. Desai et al. (2023) classified grid points where  $\mu_{ice} > 0.9$  as ice,  $0.1 \leq \mu_{ice} \leq 0.9$  as mixed phase, and  $\mu_{ice} < 0.1$  as liquid phase.

$$\mu_{ice} = \frac{IWC}{IWC + LWC} \quad (1)$$

Figures 9a–9c displays vertical profiles of the mean ice water fraction for the ERA5, JRA55, and MERRA2 reanalysis data at Scott Base derived between 2022 and 2023 inclusive. The ice water fraction is near one for ERA5 everywhere apart from the lowest 2 km of the atmosphere (see Figure 9a) which suggests that nearly all the cloud identified would be ice cloud based on the Desai et al. (2023) scheme. The ice water fraction is even larger for the JRA55 reanalysis with only the lowest altitude displaying a value which would be connected to mixed-phase cloud. Interestingly, the MERRA2 reanalysis shows much smaller ice cloud fraction values than ERA5 and JRA55, with values between 0.1 and 1.0 between the surface and 6 km, above which the mean value is one.

Figures 9d–9f display the total cloud occurrence taken directly from the reanalyses, and the cloud occurrence associated with ice and liquid water derived using the Desai et al. (2023) scheme. Comparison between the total cloud occurrence in Figures 1 and 9d–9f allows the effect of the instrument simulator to be examined. Comparison between Figures 1 and 9d shows that the raw ERA5 cloud occurrences are around 4%–5% higher than those derived after the application of the instrument simulator. This difference likely represents the impact of attenuation by low-level cloud and instrument sensitivity affects meaning that tenuous clouds will not meet the backscatter threshold used in the cloud detection scheme. Comparison between Figures 1 and 9e shows that the raw JRA55 cloud occurrences have marginally higher values than those derived using the instrument simulator; the small difference may be associated with the small quantity of low-level cloud in the JRA55 simulation. Finally, inspection of Figures 1 and 9f shows a sizable difference between the raw MERRA2 cloud occurrences and those derived from the instrument simulator. The difference is particularly large above 2 km, again likely due to instrument sensitivity factors and the simulation of the effect of attenuating low-level clouds. This comparison demonstrates the value of the use of instrument simulators in the evaluation of model output.

We now focus on the occurrence of ice and liquid water cloud, as identified by the Desai et al. (2023) scheme, in Figures 9d–9f. Notably ERA5 and JRA55 display such small quantities of liquid water that the occurrence of that cloud is barely visible relative to the zero occurrence line. Interestingly, MERRA2 displays liquid water occurrences up to approximately 2.5% below 2 km. However, these values are still considerably smaller than the occurrence of supercooled liquid cloud in Figure 8, though the fraction of liquid water to the total cloud occurrence is larger than that in Figure 8. Comparison of the ice water cloud occurrence (dashed line) and total cloud occurrence in Figure 9d shows that some mixed-phase cloud, as identified by the Desai et al. (2023) scheme, exists at altitudes below 4 km in the ERA5 data set. Similar comparison for Figure 9e shows a very small amount of mixed-phase cloud exists below 2 km in the JRA55 reanalysis. Finally, the difference between the ice cloud occurrence line and the total cloud occurrence line in Figure 9 shows that mixed-phase cloud makes up the majority of the cloud observed between approximately 2 and 5 km in the MERRA2 reanalysis.

#### 4. Conclusions and Discussion

This paper has principally detailed a comparison of CL51 ceilometer observations relative to ERA5, JRA55, and MERRA2 model output that has been processed using an instrument simulator. The application of the instrument simulator to the reanalyses output allows the derivation of pseudo-backscatter profiles, which in turn can be processed using the same cloud mask algorithm. This processing therefore allows a like-for-like comparison to be performed between the ceilometer and reanalyses output which accounts for instrumental sensitivities and differences in the way that the models represent cloud. Comparison between cloud occurrences derived from the instrument simulator (Figure 1) and those taken directly from the reanalyses (Figure 9) highlight the value of this methodology. However, it must be borne in mind that the nature of the radiative transfer calculations used in the lidar simulator mean that the impact of both the cloud phase and cloud fraction are convolved. This means that the current comparison would require both the correct quantity and the phase of cloud to be simulated by the reanalyses for the cloud occurrence to exactly match the ceilometer observations. This suggests that compensating errors which are common in models (A. Schuddeboom et al., 2019; A. J. Schuddeboom & McDonald, 2021) can be identified, but also means that identification of these errors can be more complex.

Comparison of the CL51 ceilometer vertical profiles of cloud occurrence relative to previous observations made during the AWARE campaign (Lubin et al., 2020) suggest that our low-level cloud may be underestimated because of differences in instrument sensitivity relative to the HSRL instrument they used. However, comparison with previous CALIOP–CloudSat climatologies over the Ross Ice Shelf (Jolly et al., 2018) suggests that both sets of ground-based observations measure more cloud below 2 km than the satellite observations; this result further supports the conclusions made in McErlich et al. (2021).

Critically, we find that the vertical profile of cloud occurrence for all three reanalyses shows significant underestimation below 3 km and a smaller overestimation above that altitude relative to the CL51 observations. This result can be compared qualitatively with a comparison between CAM6 simulations and the AWARE data set detailed in Yip et al. (2021) which partially attributed to low biases in humidity relative to observations. This does not appear to be the case in our study, given all three reanalyses identify overestimated relative humidity below 2 km relative to radiosonde observations in Figure 2.

Recent work detailed in Zhang et al. (2023) has identified that output from the Energy Exascale Earth System Model version 2 (EAMv2) tends to overestimate cloud frequency of occurrence throughout the year in Antarctica which differs from our results. However, they also find that cloud base height and cloud top height are much higher than observations across the year. This would suggest underestimates of cloud occurrence at low altitudes and overestimates at higher altitudes which match with the results observed in the present study. They also identify that EAMv2 tends to simulate stratiform mixed-phase clouds with significantly underestimated liquid water paths at the McMurdo station. This matches with results from the ERA5 and JRA55 reanalyses which show smaller fractions of liquid water clouds than identified in the ceilometer observations using the XGBoost scheme (Guyot et al., 2022).

Furthermore, Yip et al. (2021) highlighted a strong positive relationship between biases in cloud occurrence and relative humidity between CAM6 model output and observations made at the McMurdo station. Examination of Figures 2 and 3e–3h shows that this relationship is not identified when looking at the three reanalyses relative to the observations used in this study. In particular, the relative humidity is overestimated in all of the reanalyses relative to radiosonde observations made at the McMurdo station in the bottom 2 km of the atmosphere, while cloud occurrences are underestimated. This difference between the present study and the result in Yip et al. (2021) could be partially explained by our use of an instrument simulator which allows a more robust comparison between the cloud occurrence observations and the model output. The similar magnitudes of the underestimated and overestimated cloud occurrences below and above 3 km in Yip et al. (2021) are potentially caused by a lack of consideration of instrumental factors relative to our analysis which shows much larger biases at low altitudes. The lack of correlation between relative humidity and cloud occurrence biases at low levels for the three reanalyses suggests that the cloud occurrence biases are not associated with humidity biases in the three prognostic schemes used, but instead relate to the cloud formation parametrization themselves. While each reanalysis uses a different prognostic cloud parametrization, MERRA2 and JRA55 displayed the largest underestimates in cloud occurrence, and both their schemes examine the probability density function of total water relative to a threshold to trigger cloud formation. This result possibly suggests that these trigger levels may be inappropriately tuned for the processes occurring in the polar environment.

Further support for the robustness of the present analysis comes from results in Kuma et al. (2020), which compared ceilometer observations against the nudged HadGEM3 general circulation model and MERRA2 reanalysis output processed using the ALCF instrument simulator. In particular, the biases between the MERRA2 cloud occurrences and the ceilometer observations over the Southern Ocean were quite similar to those observed in the present study at low altitudes.

Our results also show that the CL51 ceilometer seasonal cloud occurrence and cloud fraction show little variation, similar to results in Jolly et al. (2018) and Silber et al. (2018). Notably, we find that there is a lack of a strong seasonal cycle in cloud fraction in both the CL51 ceilometer observations and the reanalyses. However, the cloud fraction is underestimated by around 25% in ERA5 and MERRA2 and by 70% in JRA55 relative to the CL51 ceilometer observations. This work thus further demonstrates the value of instrument simulators model evaluation.

Given that previous work has highlighted the importance of synoptic state on cloud properties, we derived a weather classification using a similar methodology to that detailed in McDonald and Cairns (2020). As expected,

when grouping cloud occurrence vertical profiles by weather state, mean values display much larger variability than that observed for different seasons. All three reanalyses continue to display underestimates of cloud occurrence above 3 km and overestimates above 3 km relative to the ceilometer observations for all the different nodes in our weather classification. However, the ERA5 reanalyses variability in cloud occurrence matches the changes observed in the CL51 observations for different weather states much better than the other two reanalyses. In particular, higher cloud occurrences are observed for node 1 and 4 close to 2 km and lower values in node 2 and 5. Given that much of the higher altitude cloud in this region is associated with large scale synoptic features, such as extratropical cyclones, this suggests that ERA5 represents these controlling factors better in these situations than either JRA55 or MERRA2. It is possible that our usage of the ERA5 surface wind data set to create our classification has biased our results, but given the results in McDonald and Cairns (2020) that the ERA5, MERRA2, and JRA55 surface winds are highly consistent over the satellite era, we believe this is unlikely.

Additionally, we note that the cloud occurrence is underestimated for all nodes below 2 km in all three reanalyses. Positively, vertical profiles of the cloud occurrence derived from the JRA55 and MERRA2 reanalyses do show variations in cloud occurrence which correspond with the CL51 observations, though the correspondence is much poorer than that between the CL51 observations and the ERA5 reanalysis above 2 km. While the patterns are quite consistent between the JRA55 and MERRA2 simulation results in general, the MERRA2 cloud occurrences are higher at nearly every altitude in every node than the corresponding JRA55 values. These results likely represent differences between the underlying cloud parameterizations in the different reanalyses as previously identified.

Finally, we apply a machine learning scheme developed for the classification of the cloud phase from attenuated volume backscatter coefficient data. This scheme has been developed and validated previously for polar conditions as discussed in detail in Guyot et al. (2022). While we cannot validate this algorithm at Scott Base because of a lack of polarization data, visual inspection of attenuated volume backscatter coefficient data and cloud classifications appears to confirm that this scheme works well (see Figure 7), though likely provides a conservative estimate of supercooled liquid cloud. Classification of the climatological attenuated volume backscatter coefficient data from the CL51 observations at Scott Base allows the mean occurrence of supercooled liquid water cloud to be derived. The supercooled liquid water cloud fraction remains relatively constant between 0.5 and 2.5 km at an occurrence rate of 5% and rapidly declines above that level. This pattern matches with the vertical profile identified in Silber et al. (2018), though the cloud occurrence is again lower. This suggests that these relatively inexpensive vertically pointing lidars which can be left unattended for long periods can be a valuable source of data on cloud properties in the Antarctic environment which complements satellite observations. Application of a simple classification of reanalyses output, (see details in Desai et al. (2023)), shows that ERA5 and JRA55 appear to significantly underestimate liquid-water cloud and mixed-phase cloud relative to the values derived from the CL51 observations. Liquid water and mixed-phase cloud makes up the majority of the cloud observed in the MERRA2 reanalysis below 5 km, possibly explaining the large difference between the raw cloud occurrence and the cloud occurrence derived from the instrument simulator for this reanalyses. We note that the poor estimation of the cloud phase in ERA5 identified by our results is somewhat surprising given the recent inclusion of updates detailed in Forbes and Ahlgrimm (2014) in that reanalysis.

In summary, our results highlight that the vertical profile of cloud occurrence for all three reanalyses shows significant underestimation below 3 km and a smaller overestimation above that altitude relative to the CL51 observations. The low-level biases are largest for the JRA55 reanalysis in terms of cloud occurrence and the cloud phase. The MERRA2 reanalysis displays the largest cloud occurrence biases at higher altitudes relative to the CL51 observations and appears to overestimate the proportion of supercooled liquid and mixed-phase cloud at low levels. The larger bias at higher altitudes likely offsets the low-level cloud occurrence biases in MERRA2 when cloud fraction is examined. Finally, the ERA5 cloud occurrence is significantly underestimated relative to the ceilometer observations at low levels, but displays small biases elsewhere. In particular, the ERA5 reanalysis displays an improved representation of cloud occurrence when data are grouped based on weather state relative to the other two reanalyses.

## Data Availability Statement

The ERA5 reanalyses data used in this study are available for download from the Climate Data Store (Hersbach, 2023). The JRA55, Japanese 55-year Reanalysis 3-hourly data are available from the Research Data

## Acknowledgments

AJM acknowledges the support provided by the Deep South National Science Challenge (Grant C01X1901). PK acknowledges support by the NextGEMS project funded by the European Union's Horizon 2020 research and innovation program (Grant 101003470). LW acknowledges support from the European Research Council Consolidator grant STEP-CHANGE (Grant 101045273). We also acknowledge the JRA55 data set used in this study which is provided by the Japanese 55-year Reanalysis project carried out by the Japan Meteorological Agency (JMA). We would also like to acknowledge the ERA5 reanalysis provided by the European Centre for Medium-Range Weather Forecasting. We also recognize the efforts of MDISC, managed by the NASA Goddard Earth Sciences (GES) Data and Information Services Center (DISC), who provide access to the MERRA2 data set. We would also like to thank Lee Welhouse from the Antarctic Meteorological Research and Data Center (AMRDC) who provided us with access to the McMurdo station radiosonde data used in this paper. Open access publishing facilitated by University of Canterbury, as part of the Wiley - University of Canterbury agreement via the Council of Australian University Librarians.

Archive at the National Center for Atmospheric Research, Computational and Information Systems Laboratory (JMA, 2013). The MERRA2 data are available for download from the GES-DISC (Global Modeling and Assimilation Office, 2015). The McMurdo Station Radiosonde Observations are available from <https://doi.org/10.48567/ka0n-n046>. All of the University of Canterbury ceilometer data processed using ALCF and the output from the ALCF lidar simulator derived from the various model archives (AMPS, ERA5, JRA55, and MERRA2) used in this study are accessible at Zenodo, along with code for creating all figures (<https://doi.org/10.5281/zenodo.11458722>, McDonald & Plank, 2024). The Automatic Lidar Ceilometer Framework software package is available at <https://doi.org/10.5281/zenodo.3764287> (Kuma et al., 2021).

## References

- Adhikari, L., Wang, Z. E., & Deng, M. (2012). Seasonal variations of Antarctic clouds observed by CloudSat and CALIPSO satellites. *Journal of Geophysical Research*, 117(D4), D04202. <https://doi.org/10.1029/2011jd016719>
- Alexander, S. P., & Protat, A. (2018). Cloud properties observed from the surface and by satellite at the northern edge of the Southern Ocean. *Journal of Geophysical Research: Atmospheres*, 123(1), 443–456. <https://doi.org/10.1002/2017jd026552>
- Bacmeister, J. T., Suarez, M. J., & Robertson, F. R. (2006). Rain reevaporation, boundary layer–convection interactions, and Pacific rainfall patterns in an AGCM. *Journal of the Atmospheric Sciences*, 63(12), 3383–3403. <https://doi.org/10.1175/JAS3791.1>
- Bedos-Salcedo, A., Andrews, T., Karmalkar, A. V., & Ringer, M. A. (2016). Cloud liquid water path and radiative feedbacks over the Southern Ocean. *Geophysical Research Letters*, 43(20), 10938–10946. <https://doi.org/10.1002/2016gl070770>
- Bedos-Salcedo, A., Webb, M. J., Bony, S., Chepfer, H., Dufresne, J. L., Klein, S. A., et al. (2011). COSP Satellite simulation software for model assessment. *Bulletin of the American Meteorological Society*, 92(8), 1023–1043. <https://doi.org/10.1175/2011bams2856.1>
- Bracegirdle, T. J. (2013). Climatology and recent increase of westerly winds over the Amundsen Sea derived from six reanalyses. *International Journal of Climatology*, 33(4), 843–851. <https://doi.org/10.1002/joc.3473>
- Bracegirdle, T. J., & Marshall, G. J. (2012). The reliability of Antarctic tropospheric pressure and temperature in the latest global reanalyses. *Journal of Climate*, 25(20), 7138–7146. <https://doi.org/10.1175/jcli-d-11-00685.1>
- Bromwich, D. H., Nicolas, J. P., Hines, K. M., Kay, J. E., Key, E. L., Lazzara, M. A., et al. (2012). Tropospheric clouds in Antarctica. *Reviews of Geophysics*, 50(1), 40. <https://doi.org/10.1029/2011rg000363>
- Chiriaci, M., Vautard, R., Chepfer, H., Haefelin, M., Dudhia, J., Wanherdrick, Y., et al. (2006). The ability of MM5 to simulate ice clouds: Systematic comparison between simulated and measured fluxes and lidar/radar profiles at the SIRTA atmospheric observatory. *Monthly Weather Review*, 134(3), 897–918. <https://doi.org/10.1175/MWR3102.1>
- Coggins, J. H. J., McDonald, A. J., & Jolly, B. (2014). Synoptic climatology of the Ross Ice Shelf and Ross Sea region of Antarctica: k-means clustering and validation. *International Journal of Climatology*, 34(7), 2330–2348. <https://doi.org/10.1002/joc.3842>
- Dale, E. R., McDonald, A. J., Coggins, J. H. J., & Rack, W. (2017). Atmospheric forcing of sea ice anomalies in the Ross Sea polynya region. *The Cryosphere*, 11(1), 266–280. <https://doi.org/10.5194/tc-11-267-2017>
- Delanoe, J., & Hogan, R. J. (2010). Combined CloudSat-CALIPSO-MODIS retrievals of the properties of ice clouds. *Journal of Geophysical Research*, 115(D4), D00H29. <https://doi.org/10.1029/2009jd012346>
- Desai, N., Diao, M., Shi, Y., Liu, X., & Silber, I. (2023). Ship-based observations and climate model simulations of cloud phase over the Southern Ocean. *Journal of Geophysical Research: Atmospheres*, 128(11), e2023JD038581. <https://doi.org/10.1029/2023JD038581>
- Fogt, R. L., Goergens, C. A., Jones, J. M., Schneider, D. P., Nicolas, J. P., Bromwich, D. H., & Dusselier, H. E. (2017). A twentieth century perspective on summer Antarctic pressure change and variability and contributions from tropical SSTs and ozone depletion. *Geophysical Research Letters*, 44(19), 9918–9927. <https://doi.org/10.1002/2017gl075079>
- Forbes, R. M., & Ahlgren, M. (2014). On the representation of high-latitude boundary layer mixed-phase cloud in the ECMWF global model. *Monthly Weather Review*, 142(9), 3425–3445. <https://doi.org/10.1175/mwr-d-13-00325.1>
- Frey, R. A., Ackerman, S. A., Liu, Y. H., Strabala, K. I., Zhang, H., Key, J. R., & Wang, X. G. (2008). Cloud detection with MODIS. Part I: Improvements in the MODIS cloud mask for collection 5. *Journal of Atmospheric and Oceanic Technology*, 25(7), 1057–1072. <https://doi.org/10.1175/2008tech1052.1>
- Gelaro, R., McCarty, W., Suarez, M. J., Todling, R., Molod, A., Takaes, L., et al. (2017). The Modern-Era Retrospective Analysis for Research and Applications, Version 2 (MERRA-2). *Journal of Climate*, 30(14), 5419–5454. <https://doi.org/10.1175/jcli-d-16-0758.1>
- Global Modeling and Assimilation Office. (2015). inst3\_3d\_asm\_nv: MERRA-2 3D IAU State, Meteorology Instantaneous 3-hourly, version 5.12.4 [Dataset]. *Global Modeling and Assimilation Office*. <https://doi.org/10.5067/WWQSXQ8IVFW8>
- Guyot, A., Protat, A., Alexander, S. P., Klekociuk, A. R., Kuma, P., & McDonald, A. (2022). Detection of supercooled liquid water containing clouds with ceilometers: Development and evaluation of deterministic and data-driven retrievals. *Atmospheric Measurement Techniques*, 15(12), 3663–3681. <https://doi.org/10.5194/amt-15-3663-2022>
- Haynes, J. M., Jakob, C., Rossow, W. B., Tselioudis, G., & Brown, J. (2011). Major characteristics of Southern Ocean cloud regimes and their effects on the energy budget. *Journal of Climate*, 24(19), 5061–5080. <https://doi.org/10.1175/2011jcli4052.1>
- Hersbach, H. (2023). ERA5 hourly data on pressure levels from 1940 to present [Dataset]. *Copernicus Climate Change Service (C3S) Climate Data Store (CDS)*. <https://doi.org/10.24381/eds.bd0915c6>
- Hersbach, H., Bell, B., Berrisford, P., Hirahara, S., Horányi, A., Muñoz-Sabater, J., et al. (2020). The ERA5 global reanalysis. *Quarterly Journal of the Royal Meteorological Society*, 146(730), 1999–2049. <https://doi.org/10.1002/qj.3803>
- Hofer, S., Amory, C., Kittel, C., Carlsen, T., Le Toumelin, L., & Storlmo, T. (2021). The contribution of drifting snow to cloud properties and the atmospheric radiative budget over Antarctica. *Geophysical Research Letters*, 48(22), e2021GL094967. <https://doi.org/10.1029/2021GL094967>
- Hogan, R. J., Behera, M. D., O'Connor, E. J., & Illingworth, A. J. (2004). Estimate of the global distribution of stratiform supercooled liquid water clouds using the LITE lidar. *Geophysical Research Letters*, 31(5), L05106. <https://doi.org/10.1029/2003gl018977>
- Hopkin, E., Illingworth, A. J., Charlton-Perez, C., Westbrook, C. D., & Ballard, S. (2019). A robust automated technique for operational calibration of ceilometers using the integrated backscatter from totally attenuating liquid clouds. *Atmospheric Measurement Techniques*, 12(7), 4131–4147. <https://doi.org/10.5194/amt-12-4131-2019>
- Huai, B., Wang, Y., Ding, M., Zhang, J., & Dong, X. (2019). An assessment of recent global atmospheric reanalyses for Antarctic near surface air temperature. *Atmospheric Research*, 226, 181–191. <https://doi.org/10.1016/j.atmosres.2019.04.029>

- JMA. (2013). JRA-55: Japanese 55-year reanalysis, daily 3-hourly and 6-hourly data [Dataset]. *Research Data Archive at the National Center for Atmospheric Research, Computational and Information Systems Laboratory*. Retrieved from <https://rda.ucar.edu/datasets/ds0628000/>
- Jolly, B., Kuma, P., McDonald, A., & Parsons, S. (2018). An analysis of the cloud environment over the Ross Sea and Ross Ice Shelf using CloudSat/CALIPSO satellite observations: The importance of synoptic forcing. *Atmospheric Chemistry and Physics*, 18(13), 9723–9739. <https://doi.org/10.5194/acp-18-9723-2018>
- Jung, T., Gordon, N. D., Bauer, P., Bromwich, D. H., Chevallier, M., Day, J. J., et al. (2016). Advancing polar prediction capabilities on daily to seasonal time scales. *Bulletin of the American Meteorological Society*, 97(9), 1631–1647. <https://doi.org/10.1175/BAMS-D-14-00246.1>
- Kawai, H., & Inoue, T. (2006). A simple parameterization scheme for subtropical marine stratocumulus. *SOLA*, 2, 17–20. <https://doi.org/10.2151/sola.2006-005>
- Kay, J. E., Bourdages, L., Miller, N. B., Morrison, A., Yettella, V., Chepfer, H., & Eaton, B. (2016). Evaluating and improving cloud phase in the Community Atmosphere Model version 5 using spaceborne lidar observations. *Journal of Geophysical Research: Atmospheres*, 121(8), 4162–4176. <https://doi.org/10.1002/2015jd024699>
- Kobayashi, S., Ota, Y., Harada, Y., Ebida, A., Moriya, M., Onoda, H., et al. (2015). The JRA-55 reanalysis: General specifications and basic characteristics. *Journal of the Meteorological Society of Japan*, 93(1), 5–48. <https://doi.org/10.2151/jmsj.2015-001>
- Kohonen, T. (1990). The Self-Organizing Map. *Proceedings of the IEEE*, 78(9), 1464–1480. <https://doi.org/10.1109/5.58325>
- Kremser, S., Harvey, M., Kuma, P., Hartery, S., Saint-Macary, A., McGregor, J., et al. (2021). Southern Ocean cloud and aerosol data: A compilation of measurements from the 2018 Southern Ocean Ross Sea Marine Ecosystems and Environment voyage. *Earth System Science Data*, 13(7), 3115–3153. <https://doi.org/10.5194/essd-13-3115-2021>
- Kuma, P. (2020). cl2nc [Online Multimedia]. Zenodo. <https://doi.org/10.5281/zenodo.4409716>
- Kuma, P., Bender, F. A. M., Schuddeboom, A., McDonald, A. J., & Seland, O. (2023). Machine learning of cloud types in satellite observations and climate models. *Atmospheric Chemistry and Physics*, 23(1), 523–549. <https://doi.org/10.5194/acp-23-523-2023>
- Kuma, P., McDonald, A. J., Morgenstern, O., Alexander, S. P., Cassano, J. J., Garrett, S., et al. (2020). Evaluation of Southern Ocean cloud in the HadGEM3 general circulation model and MERRA-2 reanalysis using ship-based observations. *Atmospheric Chemistry and Physics*, 20(11), 6607–6630. <https://doi.org/10.5194/acp-20-6607-2020>
- Kuma, P., McDonald, A. J., Morgenstern, O., Querel, R., Silber, I., & Flynn, C. J. (2021). Ground-based lidar processing and simulator framework for comparing models and observations (ALCF 1.0). *Geoscientific Model Development*, 14(1), 43–72. <https://doi.org/10.5194/gmd-14-43-2021>
- Lachlan-Cope, T. (2010). Antarctic clouds. *Polar Research*, 29(2), 150–158. <https://doi.org/10.1111/j.1751-8369.2010.00148.x>
- Listowski, C., Delanoë, J., Kirchgässner, A., Lachlan-Cope, T., & King, J. (2019). Antarctic clouds, supercooled liquid water and mixed phase, investigated with DARDAR: Geographical and seasonal variations. *Atmospheric Chemistry and Physics*, 19(10), 6771–6808. <https://doi.org/10.5194/acp-19-6771-2019>
- Liu, D., Liu, Q., Qi, L., & Fu, Y. (2016). Oceanic single-layer warm clouds missed by the Cloud Profiling Radar as inferred from MODIS and CALIOP measurements. *Journal of Geophysical Research: Atmospheres*, 121(21), 12947–12965. <https://doi.org/10.1002/2016JD025485>
- Lubin, D., Zhang, D., Silber, I., Scott, R. C., Kalogeris, P., Battaglia, A., et al. (2020). AWARE: The Atmospheric Radiation Measurement (ARM) West Antarctic Radiation Experiment. *Bulletin of the American Meteorological Society*, 101(7), E1069–E1091. <https://doi.org/10.1175/BAMS-D-18-0278.1>
- Marchand, R., Mace, G. G., Ackerman, T., & Stephens, G. (2008). Hydrometeor detection using Cloudsat - An earth-orbiting 94-GHz cloud radar. *Journal of Atmospheric and Oceanic Technology*, 25(4), 519–533. <https://doi.org/10.1175/2007jtecha1006.1>
- McDonald, A. J., & Cairns, L. H. (2020). A new method to evaluate reanalyses using synoptic patterns: An example application in the Ross Sea/Ross Ice Shelf Region. *Earth and Space Science*, 7(1), e2019EA000794. <https://doi.org/10.1029/2019EA000794>
- McDonald, A. J., & Plank, G. (2024). Evaluating Cloud Properties at Scott Base: Comparing Ceilometer Observations with ERA5, JRA55, and MERRA2 Reanalyses Using an Instrument Simulator (Pre-review) [Dataset]. Zenodo. <https://doi.org/10.5281/zenodo.11458725>
- McErlich, C., McDonald, A., Renwick, J., & Schuddeboom, A. (2023). An assessment of Southern Hemisphere extratropical cyclones in ERA5 using WindSat. *Journal of Geophysical Research: Atmospheres*, 128(22), e2023JD038554. <https://doi.org/10.1029/2023JD038554>
- McErlich, C., McDonald, A., Schuddeboom, A., & Silber, I. (2021). Comparing satellite- and ground-based observations of cloud occurrence over high southern latitudes. *Journal of Geophysical Research: Atmospheres*, 126(6), e2020JD033607. <https://doi.org/10.1029/2020JD033607>
- McFarquhar, G. M., Bretherton, C. S., Marchand, R., Protat, A., DeMott, P. J., Alexander, S. P., et al. (2021). Observations of clouds, aerosols, precipitation, and surface radiation over the Southern Ocean: An overview of CAPRICORN, MARCUS, MICRE, and SOCRATES. *Bulletin of the American Meteorological Society*, 102(4), E894–E928. <https://doi.org/10.1175/BAMS-D-20-0132.1>
- Nygard, T., Vihma, T., Birnbaum, G., Hartmann, J., King, J., Lachlan-Cope, T., et al. (2016). Validation of eight atmospheric reanalyses in the Antarctic Peninsula region. *Quarterly Journal of the Royal Meteorological Society*, 142(695), 684–692. <https://doi.org/10.1002/qj.2691>
- O'Connor, E. J., Illingworth, A. J., & Hogan, R. J. (2004). A technique for autocalibration of cloud lidar. *Journal of Atmospheric and Oceanic Technology*, 21(5), 777–786. [https://doi.org/10.1175/1520-0426\(2004\)021\(0777:atafc\)2.0.co;2](https://doi.org/10.1175/1520-0426(2004)021(0777:atafc)2.0.co;2)
- Pei, Z., Fiddes, S. L., French, W. J. R., Alexander, S. P., Mallet, M. D., Kuma, P., & McDonald, A. (2023). Assessing the cloud radiative bias at Macquarie Island in the ACCESS-AM2 model. *Atmospheric Chemistry and Physics*, 23(23), 14691–14714. <https://doi.org/10.5194/acp-23-14691-2023>
- Platnick, S., King, M. D., Ackerman, S. A., Menzel, W. P., Baum, B. A., Riedi, J. C., & Frey, R. A. (2003). The MODIS cloud products: Algorithms and examples from Terra. *IEEE Transactions on Geoscience and Remote Sensing*, 41(2), 459–473. <https://doi.org/10.1109/tgrs.2002.808301>
- Reid, K. J., Arblaster, J. M., Alexander, L. V., & Siems, S. T. (2024). Spurious trends in high latitude Southern Hemisphere precipitation observations. *Geophysical Research Letters*, 51(6), e2023GL106994. <https://doi.org/10.1029/2023GL106994>
- Rossow, W. B., & Schiffer, R. A. (1999). Advances in understanding clouds from ISCCP. *Bulletin of the American Meteorological Society*, 80(11), 2261–2287. [https://doi.org/10.1175/1520-0477\(1999\)080\(2261:aiuefi\)2.0.co;2](https://doi.org/10.1175/1520-0477(1999)080(2261:aiuefi)2.0.co;2)
- Sassen, K., Wang, Z., & Liu, D. (2008). Global distribution of cirrus clouds from CloudSat/Cloud-Aerosol Lidar and Infrared Pathfinder Satellite Observations (CALIPSO) measurements. *Journal of Geophysical Research*, 113(D20), 12. <https://doi.org/10.1029/2008jd009972>
- Schneider, D. P., & Fogt, R. L. (2018). Artifacts in century-length atmospheric and coupled reanalyses over Antarctica due to historical data availability. *Geophysical Research Letters*, 45(2), 964–973. <https://doi.org/10.1002/2017gl076226>
- Schuddeboom, A., Varma, V., McDonald, A. J., Morgenstern, O., Harvey, M., Parsons, S., et al. (2019). Cluster-based evaluation of model compensating errors: A case study of cloud radiative effect in the Southern Ocean. *Geophysical Research Letters*, 46(6), 3446–3453. <https://doi.org/10.1029/2018gl081686>
- Schuddeboom, A. J., & McDonald, A. J. (2021). The Southern Ocean radiative bias, cloud compensating errors, and equilibrium climate sensitivity in CMIP6 models. *Journal of Geophysical Research: Atmospheres*, 126(22), e2021JD035310. <https://doi.org/10.1029/2021JD035310>

- Scott, R. C., & Lubin, D. (2014). Mixed-phase cloud radiative properties over Ross Island, Antarctica: The influence of various synoptic-scale atmospheric circulation regimes. *Journal of Geophysical Research: Atmospheres*, 119(11), 6702–6723. <https://doi.org/10.1002/2013jd021132>
- Scott, R. C., & Lubin, D. (2016). Unique manifestations of mixed-phase cloud microphysics over Ross Island and the Ross Ice Shelf, Antarctica. *Geophysical Research Letters*, 43(6), 2936–2945. <https://doi.org/10.1002/2015gl067246>
- Seeffeldt, M. W., & Cassano, J. J. (2008). An analysis of low-level jets in the greater Ross Ice Shelf region based on numerical simulations. *Monthly Weather Review*, 136(11), 4188–4205. <https://doi.org/10.1175/2008mwr2455.1>
- Sellegrí, K., Harvey, M., Peltola, M., Saint-Macary, A., Barthelmeß, T., Rocco, M., et al. (2023). Sea2Cloud: From biogenic emission fluxes to cloud properties in the southwest Pacific. *Bulletin of the American Meteorological Society*, 104(5), E1017–E1043. <https://doi.org/10.1175/BAMS-D-21-0063.1>
- Silber, I., Fridlind, A. M., Verlinde, J., Ackerman, A. S., Cesana, G. V., & Knopf, D. A. (2021). The prevalence of precipitation from polar supercooled clouds. *Atmospheric Chemistry and Physics*, 21(5), 3949–3971. <https://doi.org/10.5194/acp-21-3949-2021>
- Silber, I., Verlinde, J., Eloranta, E. W., & Cadeddu, M. (2018). Antarctic cloud macrophysical, thermodynamic phase, and atmospheric inversion coupling properties at McMurdo Station: I. Principal data processing and climatology. *Journal of Geophysical Research: Atmospheres*, 123(11), 6099–6121. <https://doi.org/10.1029/2018JD028279>
- Smith, R. N. B. (1990). A scheme for predicting layer clouds and their water content in a general circulation model. *Quarterly Journal of the Royal Meteorological Society*, 116(492), 435–460. <https://doi.org/10.1002/qj.49711649210>
- Stephens, G. L., Vane, D. G., Tanelli, S., Im, E., Durden, S., Rokey, M., et al. (2008). CloudSat mission: Performance and early science after the first year of operation. *Journal of Geophysical Research*, 113(D23), 18. <https://doi.org/10.1029/2008jd009982>
- Swales, D. J., Pincus, R., & Bodas-Salcedo, A. (2018). The Cloud Feedback Model Intercomparison Project Observational Simulator package: Version 2. *Geoscientific Model Development*, 11(1), 77–81. <https://doi.org/10.5194/gmd-11-77-2018>
- Tastula, E. M., Vihma, T., Andreas, E. L., & Galperin, B. (2013). Validation of the diurnal cycles in atmospheric reanalyses over Antarctic sea ice. *Journal of Geophysical Research: Atmospheres*, 118(10), 4194–4204. <https://doi.org/10.1002/jgrd.50336>
- Tiedtke, M. (1993). Representation of clouds in large-scale models. *Monthly Weather Review*, 121(11), 3040–3061. [https://doi.org/10.1175/1520-0493\(1993\)121<3040:ROCILS>2.0.CO;2](https://doi.org/10.1175/1520-0493(1993)121<3040:ROCILS>2.0.CO;2)
- Trenberth, K. E., & Fasullo, J. T. (2010). Simulation of present-day and twenty-first-century energy budgets of the southern oceans. *Journal of Climate*, 23(2), 440–454. <https://doi.org/10.1175/2009JCLI3152.1>
- Vergara-Temprado, J., Miltenberger, A. K., Furtado, K., Grosvenor, D. P., Shipway, B. J., Hill, A. A., et al. (2018). Strong control of Southern Ocean cloud reflectivity by ice-nucleating particles. *Proceedings of the National Academy of Sciences of the United States of America*, 115(11), 2687–2692. <https://doi.org/10.1073/pnas.1721627115>
- Verlinden, K. L., Thompson, D. W. J., & Stephens, G. L. (2011). The three-dimensional distribution of clouds over the Southern Hemisphere high latitudes. *Journal of Climate*, 24(22), 5799–5811. <https://doi.org/10.1175/2011jcli3922.1>
- Vettigli, G. (2018). MiniSom: Minimalistic and Numpy-based implementation of the Self Organizing Map. Retrieved from <https://github.com/JustGlowing/minisom/>
- Whitehead, L. E., McDonald, A. J., & Guyot, A. (2024). Supercooled liquid water cloud classification using lidar backscatter peak properties. *Atmospheric Measurement Techniques*, 17(19), 5765–5784. <https://doi.org/10.5194/amt-17-5765-2024>
- Wiegner, M., & Gasteiger, J. (2015). Correction of water vapor absorption for aerosol remote sensing with ceilometers. *Atmospheric Measurement Techniques*, 8(9), 3971–3984. <https://doi.org/10.5194/amt-8-3971-2015>
- Winker, D. M., Vaughan, M. A., Omar, A., Hu, Y. X., Powell, K. A., Liu, Z. Y., et al. (2009). Overview of the CALIPSO Mission and CALIOP Data Processing Algorithms. *Journal of Atmospheric and Oceanic Technology*, 26(11), 2310–2323. <https://doi.org/10.1175/2009jtecha1281.1>
- Yip, J., Diao, M., Barone, T., Silber, I., & Gettelman, A. (2021). Evaluation of the CAM6 climate model using cloud observations at McMurdo Station, Antarctica. *Journal of Geophysical Research: Atmospheres*, 126(16), e2021JD034653. <https://doi.org/10.1029/2021JD034653>
- Zelinka, M. D., Myers, T. A., McCoy, D. T., Po-Chedley, S., Caldwell, P. M., Ceppi, P., et al. (2020). Causes of higher climate sensitivity in CMIP6 models. *Geophysical Research Letters*, 47(1), e2019GL085782. <https://doi.org/10.1029/2019GL085782>
- Zhang, M., Xie, S., Liu, X., Zhang, D., Lin, W., Zhang, K., et al. (2023). Evaluating EAMv2 simulated high latitude clouds using ARM measurements in the Northern and Southern Hemispheres. *Journal of Geophysical Research: Atmospheres*, 128(15), e2022JD038364. <https://doi.org/10.1029/2022JD038364>